



Toward hyper-resolution global hydrological models including human activities: application to Kyushu island, Japan

Naota Hanasaki¹, Hikari Matsuda¹, Masashi Fujiwara¹, Yukiko Hirabayashi², Shinta Seto³, Shinjiro Kanae⁴, and Taikan Oki⁵

¹Center for Climate Change Adaptation, National Institute for Environmental Studies, Tsukuba, Japan

²Faculty of Engineering, Shibaura Institute of Technology, Tokyo, Japan

³Graduate School of Engineering, Nagasaki University, Nagasaki, Japan

⁴School of Environment and Society, Tokyo Institute of Technology, Tokyo, Japan

⁵School of Engineering, University of Tokyo, Tokyo, Japan

Correspondence: Naota Hanasaki (hanasaki@nies.go.jp)

Received: 23 September 2021 – Discussion started: 28 September 2021

Revised: 28 February 2022 – Accepted: 14 March 2022 – Published: 19 April 2022

Abstract. Global hydrological models that include human activities are powerful tools for assessing water availability and use at global and continental scales. Such models are typically applied at a spatial resolution of 30 arcmin (approximately 50 km). In recent years, some 5 arcmin (9 km) applications have been reported but with numerous technical challenges, including the validation of calculations for more than 1×10^6 grid cells and the conversion of simulation results into meaningful information relevant to water resource management. Here, the H08 global water resources model was applied in two ways to Kyushu island in Japan at a resolution of 1 arcmin (2 km), and the detailed results were compared. One method involved feeding interpolated global meteorological and geographic data into the default global model (GLB; in accordance with previous high-resolution applications). For the other method, locally derived boundary conditions were input to the localized model (LOC; this method can be easily extended and applied to other regions, at least across Japan). The results showed that the GLB cannot easily reproduce the historical record, especially for variables related to human activities (e.g., dam operation and water withdrawal). LOC is capable of estimating natural and human water balance components at daily timescales and providing reliable information for regional water resource assessment. The results highlight the importance of improving data preparation and modeling methods to represent water management and use in hyper-resolution global hydrology simulations.

1 Introduction

Global hydrological models have successfully incorporated major natural hydrological components and a number of important human activities, including agricultural water use (Döll and Siebert, 2002; Wada et al., 2013), industrial and domestic water use (Alcamo et al., 2003a; Flörke et al., 2013), reservoir operation (Hanasaki et al., 2006; Shin et al., 2019), groundwater pumping (Wada et al., 2010), desalination (Hanasaki et al., 2016), and aqueduct water transfer (Hanasaki et al., 2018b). Several global hydrological models are capable of simulating global water availability and use, including most of these human activities, for the purpose of water management. Such models include WaterGAP2 (Alcamo et al., 2003a; Müller Schmied et al., 2021), LPJmL (Rost et al., 2008; Schaphoff et al., 2018), H08 (Hanasaki et al., 2008a, 2018b), WBMplus (Wisser et al., 2010), PCR-GLOBWB (Wada et al., 2011; Sutanudjaja et al., 2018), HiGW-MAT (Pokhrel et al., 2012; Shin et al., 2019), VIC5 (Droppers et al., 2020), and the Community Water Model (CWatM; Burek et al., 2020). These models have been widely employed for water scarcity assessment (Alcamo et al., 2003b; Hanasaki et al., 2018a), climate change impact assessment (Schewe et al., 2014), water footprinting (Hanasaki et al., 2010; Dalin et al., 2017), estimation of the Earth's carrying capacity (Gerten et al., 2020), and many other purposes.

Among various challenges facing global hydrological models, increasing spatial resolution is perhaps the most straightforward and most difficult. For the past decade, most global hydrological simulations have been conducted at a spatial resolution of 30 arcmin (0.5° , approximately 55 km at the Equator). A widely recognized goal is to realize a spatial resolution of 30 arcsec (approximately 1 km at the Equator), the designated hyper-resolution for global land surface modeling, which has been described by Oki et al. (2006) and Wood et al. (2011). With increased spatial resolution, human activities become non-negligible, as they predominate in highly developed and densely populated regions. The establishment of methodologies to incorporate human activities at such a scale is urgently needed.

Recently, some models have been applied at spatial resolutions considerably finer than 30 arcmin. To the authors' knowledge, the first example was reported by Eisner and Flörke (2015). They developed the WaterGAP3 model, based on WaterGAP2 (Alcamo et al., 2003a), and applied it globally at 5 arcmin resolution. Wada et al. (2016) applied the PCR-GLOBWB model globally at 6 arcmin spatial resolution. They estimated sector-wise water usage, along with the supply of surface and groundwater, and then calculated a conventional water stress index as the ratio of usage to supply. They found that water stress is unrealistically concentrated in grid cells containing the downtown areas of the largest cities (e.g., Paris and New York) and therefore recommended assessment across larger spatial domains, such as subbasins and counties. Sutanujaja et al. (2018) developed PCR-GLOBWB2 as an upgrade of PCR-GLOBWB, which has two standard spatial resolutions, i.e., 30 and 5 arcmin. They reported that the latter resolution outperformed the former, mainly due to better representation of snow processes by its more detailed air temperature distribution in mountainous areas. Burek et al. (2020) developed a new global hydrological model called CWatM, and it is based on PCR-GLOBWB and LISFLOOD (De Roo et al., 2000). Although no detailed results were reported, similar to PCR-GLOBWB2, boundary conditions for 5 arcmin resolution have been determined for this model.

Although several successful applications have been described, global hydrological modeling at scales finer than 30 arcmin is still in its infancy. Such modeling efforts face three major challenges. The first challenge is validation. To demonstrate that the models are capable of operating at a certain spatial resolution, reliable observations must be collected in advance. However, aside from river discharge, reliable global observations of hydrological variables are challenging to obtain, especially in the form of fine-scale data for water use and management. The second challenge is model refinement. To express site-specific hydrological processes and water use practices, parameter regionalization (Beck et al., 2016; Yoshida et al., 2021) and model and data localization processes are required, and these processes can easily become unmanageable unless conducted systematically and

strategically. The third challenge is the inter-grid-cell connection. Because water supply and drainage systems for urban and irrigation water distribution typically cover a greater extent than the 5 arcmin grid cell, interconnections must be considered.

To investigate the applicability of a global hydrological model at a fine spatial resolution, we applied the latest version of the H08 global hydrological model (Hanasaki et al., 2018b) to Kyushu island, Japan, at 1 arcmin spatial resolution (approximately 2 km at the Equator). The study area provides sufficient quantity and quality of data for simulation and validation with reasonable efforts. The site includes major rivers, dams, irrigation projects, active industries, and densely populated cities, providing good example locations for the application of the hyper-resolution global hydrological model. Similar efforts have been reported by Mateo et al. (2014) and Masood et al. (2015), who applied H08 at 5 arcmin spatial resolution to the Chao Phraya River in Thailand and the Ganges–Brahmaputra–Meghna rivers of the Indian subcontinent, respectively. The present study uses the latest H08 model at a 5 times higher resolution than previous works, with a focus on water management and use. Throughout this study, we assess water resources in terms of whether water is available when and where it is needed. Other assessments, such as flood risk, are outside the scope of this research. The present study addresses the following three questions. How well can the default global H08 reproduce the hydrology and water management of Kyushu island? Does the localization of the data and model improve the performance? What is the benefit of conducting hyper-resolution hydrological modeling from the viewpoint of water resources management and assessment?

2 Study area

Kyushu is the third largest island in Japan, with an area of 36 750 km². Kyushu is surrounded by the Sea of Japan to the north, the East China Sea to the west, and the Pacific Ocean to the south. The terrain is mountainous, and flat areas are mostly located along the downstream reaches of major rivers. All of Kyushu experiences a humid subtropical climate (Cfa in the Köppen–Geiger climatic classification). Mean annual precipitation is approximately 1600–2500 mm yr⁻¹ and generally increases southward. The precipitation is concentrated from June to July, when a seasonal rain front crosses the island. Additionally, typhoons occasionally bring considerable rainfall from June to October. It snows only occasionally. Because of its mountainous topography, the catchment areas of the rivers on Kyushu are relatively small. The largest river basin is the Chikugo River in north–central Kyushu, which is 143 km in length, with a basin 2860 km² in area.

In this study, we targeted nine rivers with catchment areas exceeding 1000 km² (Table 1). A total of 420 reservoirs are listed in the dam handbook issued by the Japan Dam Foun-

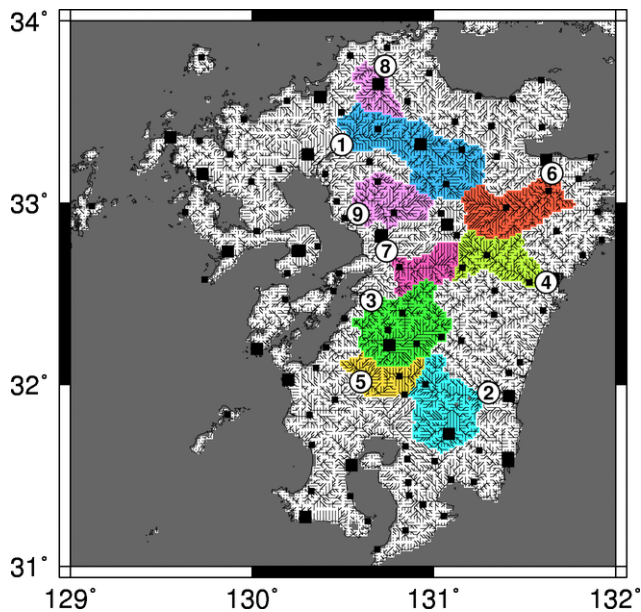


Figure 1. Study domain. Large and small squares represent manned and automated weather stations, respectively. Numbers in circles indicate gauging stations along major rivers. See Table 1 for a list of rivers and gauging stations. Colored areas are the catchment areas of the gauging stations. Numbers in triangles indicate dams located on the major rivers. See Table 2 for a list of the dams.

dation (http://damnet.or.jp/Dambinran/binran/TopIndex_en.html, last access: 11 April 2022). Due to the steep terrain of Kyushu, the storage capacity of dams on the island is relatively small. We primarily targeted 13 existing dams with a storage capacity exceeding $40 \times 10^6 \text{ m}^3$. Among these dams, eight are located in the nine major river basins included in this study (Table 2). Kyushu has seven prefectures, with a total population of 12930×10^3 in 2015 (<https://www.e-stat.go.jp/en>, last access: 11 April 2022). The total cropland area is 5500 km^2 . The dominant crop types are paddy rice and a variety of vegetables and fruits. Total water withdrawal on the island is $9.8 \text{ km}^3 \text{ yr}^{-1}$, of which $7.3 \text{ km}^3 \text{ yr}^{-1}$ is used for irrigation (Ministry of Land Infrastructure Transportation and Tourism, MLIT, 2021).

3 Methods

In this study, we applied the global hydrological model H08 (Hanasaki et al., 2018b) to Kyushu island in Japan at a spatial resolution of 1 arcmin. We ran the H08 in the following two ways: using the standard global model and using a modified model. H08 requires two types of boundary conditions, namely meteorological information at daily intervals and static geographic information. Boundary conditions were also prepared in two ways. The first set of conditions was obtained using global data. We attempted to find data at 1 arcmin or finer resolution, but most data were available

Table 1. Major rivers of Kyushu island. The gauging stations are the official reference points of rivers, where a long-term streamflow record is obtained for the planning of water management and development, with two exceptions. The official reference point for the Chikugo River is Arase (1443 km^2) but, for wider coverage of the catchment, we used the downstream station of Senoshita. Similarly, the Sendai River is recorded at Sendai (1425 km^2), but because that site is affected by the operation of the Tsuruda Dam, we used the upstream station of Suzunose.

ID	River	Catchment area (km^2)	Gauging station	Catchment area (km^2)
1	Chikugo	2860	Senoshita	2295
2	Oyodo	2230	Takaoka	1564
3	Kuma	1880	Yokoishi	1856
4	Gokase	1820	Miwa	1044
5	Sendai	1600	Szunose	720
6	Ono	1465	Shiratakibashi	1381
7	Midori	1100	Jonan	681
8	Onga	1026	Hinodebashi	695
9	Kikuchi	996	Tamana	906

Table 2. Major dams along the rivers included in this study. We excluded the Ryumon Dam due to a lack of historical observation data. We excluded the Matsubara Dam because it is located just below the Shimouke Dam, complicating its use for validation.

ID	Name	River	Capacity (10^6 m^3)
1	Shimouke	Chikugo	59.3
2	Midorikawa	Midorikawa	46.0
3	Tsuruda	Sendai	123.0
4	Ichifusa	Kuma	40.2
5	Kitagawa	Gokase	41.0
6	Iwase	Oyodo	57.0
–	Ryumon	Kikuchi	42.5
–	Matsubara	Chikugo	54.6

only at 5 arcmin or coarser resolution, which we linearly interpolated into 1 arcmin data. The second method for obtaining boundary conditions employs local data from Japanese governmental agencies and other sources, which are compiled into 1 arcmin resolution. The combination of the default model with global boundary conditions is the current typical implementation of global hyper-resolution simulations, while the localized model with local boundary conditions represents an ideal implementation when data accessibility issues have been resolved (i.e., assuming hydrometeorological data are available at high resolution for any location worldwide).

3.1 Model

3.1.1 The H08 model

H08 was originally developed to simulate the global hydrological cycle with major human activities for advanced water resource assessment at the global scale (Hanasaki et al., 2008a, 2018b). The model is grid based, and its standard spatial resolution is 30 arcmin, but it was designed for application to any spatial domain and resolution. The model consists of six submodels, namely land surface hydrology, river routing, crop growth, water abstraction, reservoir operation, and environmental flow. These components enable simulation of water availability and use at daily intervals in a fully consistent manner and division of the water used by three sectors (agricultural, industrial, and municipal) into five surface water sources (river, aqueduct, local reservoir, seawater desalination, and unspecified surface water, which is defined below) and two groundwater sources (renewable and non-renewable groundwater).

The crop growth and water abstraction submodels are detailed below, as they play particularly important roles in this study. The crop growth submodel estimates the daily growth of crops using the heat unit approach and biomass accumulation based on photosynthesis. The formulation of this submodel is identical to the widely used Soil and Water Assessment Tool (SWAT; Arnold et al., 2012). The crop growth submodel has two functions in H08. First, it is a component of H08 that outputs crop-related variables fully consistent with global water cycle simulation, such as crop yield. Second, it is a standalone model for estimating the crop calendar in the study area. Crop calendars, specifically planting and harvesting dates, are essential for determining the timing of irrigation, but local information is difficult to obtain at any scale, as these dates are rarely monitored and recorded. The principal purposes of the standalone simulation were to iterate the crop yield estimation 365 times by shifting the planting date from 1 January to 31 December in all grid cells and, thereby, to identify the date that results in the maximum crop yield.

The water abstraction submodel also plays an essential role in H08. The fundamental concept used for modeling of each water source is explained below. Water abstraction from rivers indicates the removal of a portion of the streamflow to meet the water requirement within a grid cell. Streamflow is estimated by accumulating runoff through the river network. Water abstraction from an aqueduct indicates transfer of streamflow beyond a grid cell through the artificial aqueduct network. This network is defined either explicitly (i.e., manual connections are made between source and destination grid cells) or implicitly (i.e., the origin and destination of aqueducts is inferred by assuming gravitational water transfer via an algorithm; see Hanasaki et al., 2018b, for details). Water abstraction from a local reservoir indicates abstraction of water stored in relatively small reservoirs or irrigation ponds within a grid cell that does not affect the streamflow of

the river network. Note that large reservoirs are incorporated into the river network and directly regulate streamflow. Water abstraction from seawater desalination indicates abstraction of water processed in desalination plants, which is possible only in designated regions. Water abstraction from unspecified surface water indicates the volume of the daily water requirement that was from the sources listed above; it indicates that the water requirement was not met (i.e., water deficit) or that errors occurred in simulation (e.g., underestimation of runoff, overestimation of demand, or misrepresentation of water infrastructure). Water abstraction from renewable groundwater indicates water abstraction from the groundwater reservoir of the cell, which can be recharged. Abstraction from non-renewable groundwater indicates deep groundwater pumping after the depletion of the groundwater reservoir. For simplicity, we excluded local reservoirs and seawater desalination from this study. Thus, the water requirement is divided into river, aqueduct, unspecified surface water, renewable groundwater, and non-renewable groundwater.

3.1.2 Land surface hydrology submodel localization

To reflect basin characteristics more accurately, we localized some submodels of the original H08 model. For the land surface submodel, we tuned the hydrological parameters. Numerous methods have been proposed for the tuning of parameters in hydrological models, and we adopted a simple Monte-Carlo-based method described previously (Mateo et al., 2014; Masood et al., 2015). This process identifies the combination of four sensitive hydrological parameters that minimize the Nash–Sutcliffe efficiency (NSE; Nash and Sutcliffe, 1970) of the daily streamflow simulation among three possible values for each parameter (total $3^4 = 81$ parameter sets), namely the default, upper, and lower values (see the text and Table S1 in the Supplement). We applied this method at nine major river gauging stations (Table 1). This approach is applicable to gauged basins but not ungauged basins. To tackle this problem, we identified the most frequently selected value for each parameter as the best option for application across all of Kyushu island. Then, we used the selected parameter values throughout the period and in all grid cells.

3.1.3 Reservoir operation submodel localization

The reservoir operation submodel incorporated into H08 employs simple reservoir operation rules to determine daily water release and storage for individual reservoirs from limited globally available information (Hanasaki et al., 2006). The validity of the original algorithm as a generic global model has been demonstrated in numerous previous works (Masaki et al., 2017; Yassin et al., 2019; Shin et al., 2019; Turner et al., 2020). The original reservoir operation submodel (see Hanasaki et al., 2006) releases water at a constant rate throughout the year at a rate equivalent to the mean an-

nual inflow. This process results in increased storage during the wet season and reduced storage in the dry season. When no other control is applied for subannual operation, storage can reach the storage capacity of the reservoir (and then begin to overflow) or become completely depleted (so that release becomes identical to inflow), which seldom occurs in reality (Masaki et al., 2017).

To enable more realistic behavior, we added the release curve and the upper and lower storage curves to the model (Fig. 2). The release curve assigns different release rates for the wet and dry seasons. The upper and lower storage curves determine the maximum and minimum storage in a year. The storage curves are subdivided into four phases, namely maintaining high storage, releasing, maintaining low storage, and recharging. In the releasing phase, the maximum and minimum storage values are gradually decreased to avoid a sudden increase in water release. In the recharging phase, the maximum and minimum storage values are increased to allow fast and effective recovery. The release curve is also subdivided into four phases, namely the dry season, dry to wet transition, the wet season, and wet to dry transition. To represent the various shapes of release and storage curves, we constructed a generic curve, as shown in Fig. 2. To represent these curves, we specified four points (R1–4; in time and release coordinates) on the release curve, and a total of eight points (U1–4 and L1–4; in time and storage coordinates) on the upper and lower curves. R1–4 were determined from the long-term mean monthly release levels of individual reservoirs. U1–4 and L1–4 were determined from the actual operation curves compiled by reservoir operators. Storage curves of reservoirs managed by central and local governments and public agencies are disclosed due to legislation in Japan. The parameter values used for the six dams are listed in Tables S3–5.

3.1.4 Implicit aqueduct estimation

In reality, to abstract streamflow for water use, water is withdrawn at weirs and transferred directly to the point of use (e.g., irrigated cropland) or to water treatment facilities and then supplied to urban areas through pipelines. Because the identification of weirs and manual delineation of water transfer routes is infeasible for large study domains, H08 can infer the route of inter-grid-cell gravity-based water transfer (Hanasaki et al., 2018b). The original algorithm was designed to work at a resolution of 30 arcmin, and therefore, we modified it for better performance at a fine spatial resolution.

We modified two components of this algorithm. First, the original method allows transfer of only one grid cell ahead but was modified to allow transfers a maximum of five grid cells ahead (approximately 10 km). Next, interbasin transfer was not possible in the original model but was allowed in this study if the catchment area of the destination is smaller than two grid cells. This modification adds flexibility for water transfer, especially in grid cells near coastlines, where

basins are generally small (Fig. 3). Along with these implicit aqueducts, the origins and destinations of known major water transfer facilities (designated explicit aqueducts' see Sect. 3.2.) were prepared and implemented into the river network (Fig. S1; Table S6). These explicit aqueducts transfer water irrelevant to elevation.

3.2 Data

3.2.1 Meteorological data

To run the H08 model, the following seven meteorological variables must be supplied at daily intervals: precipitation, air temperature, humidity, wind speed, surface pressure, precipitation, and downward longwave and shortwave radiation. We prepared the data using two methods, including one based on global data representing the current practice in high-resolution global modeling and one using local data.

For the global data, we extracted and linearly interpolated the WFDEI global meteorological dataset (Weedon et al., 2014) for the study domain. The dataset contains all seven variables at daily intervals from 1979–2016. WFDEI is a hybrid product of monthly observation-based global gridded meteorological data, for example, CRU TS3.1 (Climatic Research Unit gridded Time Series v3.1; Harris et al., 2014) and the Global Precipitation Climatology Centre (GPCC; Schneider et al., 2014) and the ERA-Interim daily global reanalysis data (Dee et al., 2011).

For local data, we used published meteorological records. Kyushu island contains 44 observatories (district and local meteorological observatories) and 121 automatic weather stations (Automated Meteorological Data Acquisition System – AMeDAS; <https://www.jma.go.jp/jp/amedas/>, last access: 11 April 2022) operated by the Japan Meteorological Agency (Fig. 1). AMeDAS monitors air temperature, wind speed, precipitation, and sunshine duration. Sunshine duration was converted into downward shortwave radiation using the method described in Appendix A. The observatories also monitor surface pressure and specific humidity. A total of 117 observatories and AMeDAS stations that provide continuous records were used for this study. The daily observations at observatories and stations were interpolated using inverse distance weighting and converted into grid data. Finally, downward longwave radiation was estimated using the method described in Appendix B.

3.2.2 Geographic data – hydrology

For H08, the boundary conditions listed in Table 3 must be provided. We first prepared all of these parameters by extracting and interpolating their values from the default global simulation or using the functions of H08, which were described in detail by Hanasaki et al. (2018b). Then, we prepared another set of data, utilizing local information whenever possible, as detailed below.

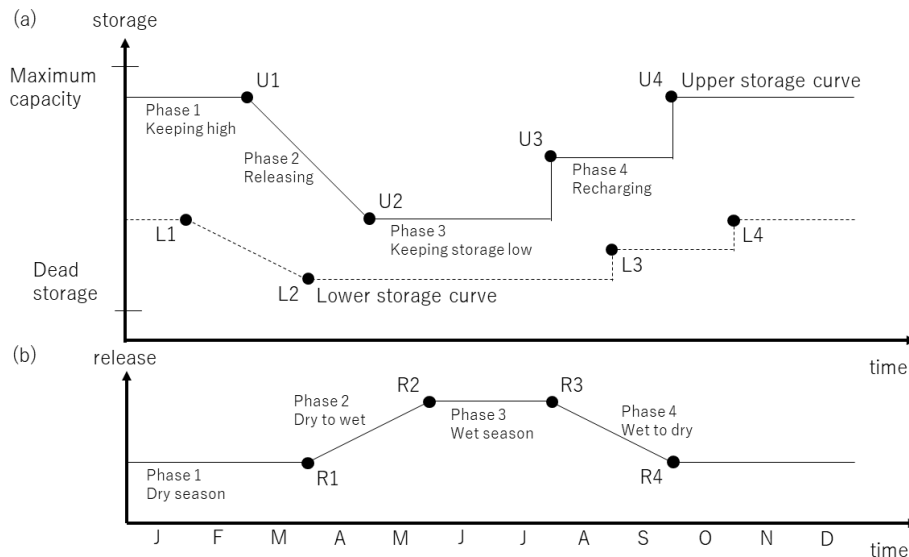


Figure 2. Schematic diagrams of (a) the upper and lower storage curves and (b) the release curve.

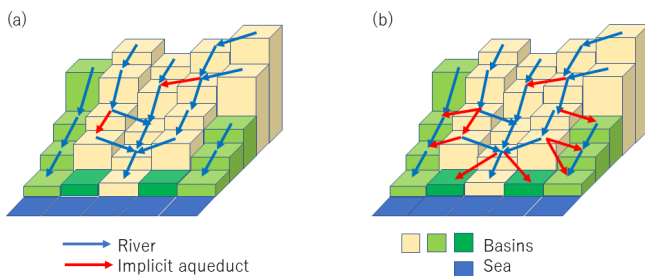


Figure 3. Implicit aqueducts. (a) The original scheme, which does not allow interbasin transfer. Many coastal grid cells (shown in dark green) are prone to water scarcity because they have a limited catchment area. (b) The new scheme which conditionally allows interbasin transfer. Coastal grid cells receive interbasin water transfer from neighboring basins. Columns represent land grid cells. The height indicates each grid cell's mean elevation. Colors indicate different basins.

We first developed a flow direction map of Kyushu island. We used the digital elevation model SRTM30_PLUS (Becker et al., 2009). Using geographic information systems (Esri ArcGIS and Arc Hydro), we constructed a flow direction map at 1 arcmin resolution. Then, we georeferenced the six largest dams, which are listed in Table 2, to the flow direction map. Next, we prepared an implicit aqueduct network with the localized algorithm (Sect. 3.1.4). We also prepared an explicit aqueduct network by identifying major weirs and manually digitizing their channels (Sect. 3.1.4).

3.2.3 Geographic data – agriculture

We adopted the data of Kohyama et al. (2003) for the distributions of crop land, crop type, and irrigated area, which are crucial factors in this simulation. They developed these data by combining National Land Numerical Information (NLNI) provided by the Ministry of Land Infrastructure and Transportation (MLIT) with the census of agriculture and forestry (CAF; <https://www.maff.go.jp/e/data/stat/>, last access: 11 April 2022) by the Ministry of Agriculture, Forestry, and Fisheries (MAFF). NLNI is the fundamental grid-based digital land use map for Japan, which is available at 1 km and 100 m spatial resolutions. One drawback of NLNI is that the cropland area reported in NLNI differs considerably from ground-based agricultural surveys due to issues with land use classification and spatial resolution (Kohyama et al., 2003). The CAF is the most comprehensive agricultural survey in Japan; it is conducted every 5 years, with the latest census conducted in 2015 and published in 2017. CAF is based on interviews with individual farmers and agricultural industries and summarized for each agricultural village, which number approximately 140 000. Although comprehensive and precise, CAF is not available in a grid-based format. Kohyama et al. (2003) scaled NLNI so that the total areas of paddy and upland crops agree with those in CAF for every agricultural village from 1970 to 1995. Unfortunately, for technical reasons, the data developers have stopped updating the dataset since then. Although outdated, we either used the gridded data for 1995 or the latest available data in this study. The spatial resolution is 45" × 30" (equivalent to approximately 1 km × 1 km). The number of crop types is 13, including rice, barley/wheat, other cereals, root vegetables, green vegetables, legumes, flowers, seeds, fodder, or-

Table 3. Geographic data used in this study.

Category	Variable	Global	Local
Hydrology	Flow direction	Same as local	Derived from the global elevation data of Becker et al. (2009)
	Locations of dams	Same as local	Japan Dam Foundation (Table 2)
	Locations of aqueducts (implicit)	Derived from the original H08 algorithm (Hanasaki et al., 2018b)	Derived from the localized algorithm (Sect. 3.1.4)
	Locations of aqueducts (explicit)	Not applicable	Localized data (Sect. 3.1.4)
Agriculture	Distribution of cropland area	Ramankutty et al. (2008)	Kohyama et al. (2003)
	Distribution of crop type	Monfreda et al. (2008)	Kohyama et al. (2003)
	Distribution of irrigated area	Siebert et al. (2005)	Kohyama et al. (2003)
	Crop calendar	Derived from the original H08 algorithm (Hanasaki et al., 2008a)	Localized data (Sect. 3.2.3)
	Irrigation efficiency	Döll and Siebert (2002)	Localized data (Sect. 3.2.3)
	Groundwater fraction of irrigation	Siebert et al. (2010)	Same as global
Municipal	Industrial water withdrawal	Food and Agriculture Organization (https://www.fao.org/aquastat/en/ , last access: 11 April 2022)	Ministry of Economy Trade and Industry (METI; 2018)
	Domestic water withdrawal	Food and Agriculture Organization (https://www.fao.org/aquastat/en/ , last access: 11 April 2022)	Japan Water Works Association (JWWA; 2018)
	Groundwater fraction of industrial water	International Groundwater Resources Assessment Centre (https://www.igrac.nl/ , last access: 11 April 2022)	Ministry of Land Infrastructure Transportation and Tourism (MLIT; 2021)
	Groundwater fraction of domestic water	International Groundwater Resources Assessment Centre (https://www.igrac.nl/ , last access: 11 April 2022)	Ministry of Land Infrastructure Transportation and Tourism (MLIT; 2021)

chards, tea, cash crops, including sugar cane and sugar beet, and other crops.

The default H08 model subdivides the grid cells into four land use types, namely double-crop irrigated cropland (for warm regions only), single-crop irrigated cropland, rainfed cropland, and non-cropland (Fig. 4a). The primary and secondary crop types are assumed to be cultivated across the entire grid cell (Hanasaki et al., 2008a). In this study, we first subdivided cropland into two categories, paddy and upland, as irrigation water use differs sharply between these two farming methods. Then, we subdivided the grid cells into five land-use types with specific crop rotations, namely double-crop irrigated paddy (rice and barley), single-crop irrigated paddy (rice), single-crop irrigated upland (summer crop), rainfed upland (summer crop), and non-cropland (Fig. 4b). The crop parameters of the crop growth submodel were taken from SWAT (Arnold et al., 2012). We used the generic values for summer crop.

To estimate the crop calendars of three crops, we used the standalone crop growth submodel (see Sect. 3.1.1). In previous global applications of H08, the estimated calendar of major crops agrees well with the reported calendar, which supports the validity of this approach. However, in application to Kyushu, we noted that special treatment is needed for rice. The H08 model estimates the optimal planting date for rice as being early May for most areas of Kyushu. However, the actual cropping practice indicates planting in early June. Therefore, we shifted the planting date of rice by 30 d. For other crops, we used the estimated crop calendar as provided.

Irrigation efficiency is defined as the rate of water consumption (i.e., evapotranspiration) to total water withdrawal. In general, irrigation efficiency is determined by irrigation equipment (i.e., high efficiency for drip irrigation and low efficiency for flood irrigation). Döll and Siebert (2002) adopted this approach and proposed a value of 0.35 for East Asia. Through comparison between simulation results and local

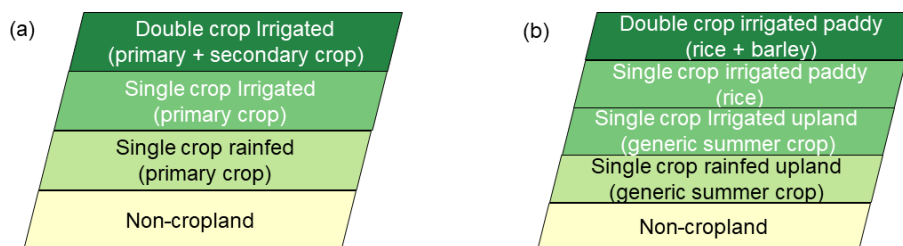


Figure 4. Grid cell categorization, with (a) the original categorization for the global mode and (b) the new categorization for the localized mode.

observations (reported in Sect. 4.1.2), we obtained a value of 0.45 for surface irrigation in this study, which is by far the predominant irrigation type used on Kyushu island. Last, for the fraction of irrigation obtained from groundwater, we were unable to find reliable statistics that cover the entire island. Therefore, we did not prepare local data and used only the global dataset (Siebert et al., 2010).

3.2.4 Geographic data – municipal

Industrial water withdrawal is provided as a census (Ministry of Economy Trade and Industry – METI, 2018). The finest geographical data are provided at the prefecture level and are further divided into 24 industrial classes. As the prefecture level is too crude (with seven in the study domain), we downscaled the data to the municipality level (numbering 233) through weighting by the value of exports, which is available for each municipality and industrial class. Finally, gridded industrial water withdrawal data were developed by assuming that the spatial distribution of water usage is proportional to population (Statistic Bureau of Japan, 2017). All data were prepared for the year 2015 to maintain consistency between municipality-based and grid-based data.

Domestic water withdrawal data were obtained from the Waterworks Statistics (Japan Water Works Association – JWWA, 2018). As the finest resolution available was the prefecture level, gridded data were developed in a manner similar to that of industrial water. The fraction of groundwater withdrawal for industrial and domestic use was obtained from the yearbook (Ministry of Land Infrastructure Transportation and Tourism – MLIT, 2021). These data are available only at the regional scale (Kyushu island is subdivided into two regions) for the industrial and domestic sectors (data for the agriculture sector are not available).

3.2.5 Validation data (streamflow, reservoir operation, and irrigation)

To validate the major outputs, we collected the observational data listed in Table 4. We used the water information system (<http://www1.river.go.jp/>, last access: 11 April 2022) of the Ministry of Land Infrastructure and Transportation (MLIT) for daily river discharge and dam operation data (i.e., release,

inflow, and storage). In cases where storage is provided only as water level, the value was converted into volume by fitting a quadratic function to the storage and water level relationship at the total, effective, and dead storage levels, which are publicly disclosed.

Daily irrigation water withdrawal is not published in Japan. We requested daily irrigation water withdrawal data from the Kyushu Regional Agricultural Administration Office (KRAAO) of the Ministry of Agriculture, Forestry, and Fisheries (MAFF). KRAAO kindly provided the daily irrigation water withdrawal data for 18 weirs in seven national irrigation projects on Kyushu, for 11 years, from 2007 to 2018. The data were provided under following conditions: first, the location of the weirs shall not be disclosed. Second, the raw data shall not be published in any document. Third, the redistribution of data shall not be permitted for any reason. Due to these conditions, we hereafter refer to the irrigation projects as A–G.

3.3 Simulation and analysis

H08 was set up at 1 arcmin spatial resolution and applied to Kyushu island (Fig. 1). Simulation was conducted for 20 years from 1995 to 2014. Due to the availability of irrigation water withdrawal data, we primarily analyzed the results of the final 8 years (2007 to 2014). Calibration of hydrological parameters was performed using simulation results for 2001–2006. We conducted the following two simulations: a global simulation (hereafter GLB), which involved running the H08 model at a high spatial resolution using the default model and interpolated standard global data and the localized simulation (LOC), which uses localized H08 model with localized boundary conditions (Table 5).

We conducted LOC variant simulations to investigate the effects of the aqueduct settings. Due to substantial differences in water availability (i.e., streamflow) and water demand (affected by irrigated area and population) among grid cells, inter-grid water transfer plays a crucial role in balancing these terms. We conducted simulations with different settings for aqueducts and examined the effect on the simulation results. LOC-II employs only the original implicit aqueduct algorithm. Aqueducts transfer water to only one downstream grid cell (approximately 2 km). Because traditional weirs and

Table 4. Validation data. MLIT and MAFF represent the Ministry of Land Infrastructure, and Transportation and the Ministry of Agriculture, Forestry, and Fisheries, respectively.

Submodel	Variables	Source
Land/river	River discharge	Water information system, MLIT
Reservoir	Reservoir inflow	Water information system, MLIT
	Reservoir release	Water information system, MLIT
	Reservoir storage	Water information system, MLIT
Crop growth/ water withdrawal	Irrigation water withdrawal	Data request from MAFF

canal systems can transfer water across several to dozens of kilometers, LOC-I5 extends the maximum reach of implicit aqueducts to five grid cells (9 km). Water-insufficient grid cells tend to occur in coastal zones, where the catchment area is rather limited but heavily populated. LOC-I5O allows water transfer outside of the basin, as illustrated in Sect. 3.1.4. Finally, LOC-I5OE includes explicit aqueducts (i.e., major weirs and municipal water systems; listed in Table S6).

4 Results

4.1 Validation

4.1.1 Discharge

Simulated daily river discharge at Senoshita on the Chikugo River is shown in Fig. 5 (results for other stations are shown in Fig. S2). Monthly river discharge obtained from LOC simulations reproduced historical observations well throughout the simulation period. Aspects of the timing and the magnitude of the largest peaks in July and some minor ones, as well as the magnitude of discharge in dry months, were similar to the observations. Daily river discharge also agreed with the observations for both wet and dry years (i.e., the years with minimum and maximum annual rainfall in the validation period), but the simulated peaks tended to be underestimated, especially with respect to minor peaks during the dry period (e.g., from September to May 2012). Monthly river discharge from GLB simulations also agreed with the observations, but the daily results show considerable discrepancies. The magnitude of peaks does not match the observed levels, and the duration of high discharge is apparently longer than the observed period (i.e., the shape of curves is flattened) after a prolonged precipitation event in the GLB simulation (not shown).

The results for other basins showed a similar general tendency (Fig. S2). The results from LOC for both monthly and daily simulations reproduced the observations. GLB performed moderately well for monthly simulations but poorly for daily simulations. The NSE values (Nash and Sutcliffe, 1970) of all seven rivers are shown in Table 6. The NSE

of LOC consistently exceeded 0.6, while all values for GLB were below 0.4.

We speculate that the difference in performance between the two simulations is due to the quality of precipitation data. Although the hydrological parameters of LOC were selected from 81 possible combinations, their effect is limited because only one parameter set was applied across the entire study domain (Sect. 3.1.2). The daily variation in precipitation for GLB is based on the ERA-Interim global reanalysis product with a resolution of approximately 45×45 arcmin (Dee et al., 2011), which is too crude to obtain 1 arcmin spatial data. The variations used for LOC are based on daily precipitation records from 117 rain gauges for the study domain of $36\,750 \text{ km}^2$, which is equivalent to approximately one rain gauge per 10×10 arcmin square. This high density of observations provided accurate information for the magnitude and timing of each rainfall event. To investigate this speculation, a systematic sensitivity simulation for river discharge was conducted (Appendix C).

4.1.2 Irrigation water requirement

Figure 6 shows the estimated irrigation water demand at irrigation project A (results for the other six sites are shown in Fig. S3). The simulated monthly water requirement of LOC was overestimated by a factor of 2, but the duration of the irrigation and its temporal variations agreed well with observed water withdrawal. GLB had a similar performance to LOC in terms of magnitude, but as discussed above, the irrigation period begins and ends earlier than the observed period by 1 month.

The daily water requirement results for 2007 and 2010 highlight the differences between the two simulations. First, the daily variations in the water requirement are much closer to reality for LOC than for GLB. This difference is due to the meteorological data and hydrological parameters used for each simulation. For example, the smaller τ of LOC (the time constant of interflow; see Sect. S1.1 in the Supplement) is associated with the overall faster drainage than GLB, which requires a greater volume of daily irrigation to maintain paddy fields without reference to precipitation events. Second, the observed water requirement shows distinct patterns, with low

Table 5. Simulations. Key differences between the GLB and LOC simulations.

	GLB	LOC
Full name	Global	Localized
Source of daily meteorological data	The ERA-Interim reanalysis (Dee et al., 2011)	Local meteorological observations (AMeDAS)
Spatial resolution of daily meteorological data	45 arcmin	10 arcmin*
Geographic data	Global boundary conditions (Table 3)	Local boundary conditions (Table 3)
Hydrological parameters	Default	Localized (Sect. 3.1.2)
Model	Default	Localized (Sect. 3.1.3–3.1.4)

* A total of 117 rain gauges for the study domain of 36 750 km², which is equivalent to approximately one rain gauge per 10 × 10 arcmin square.

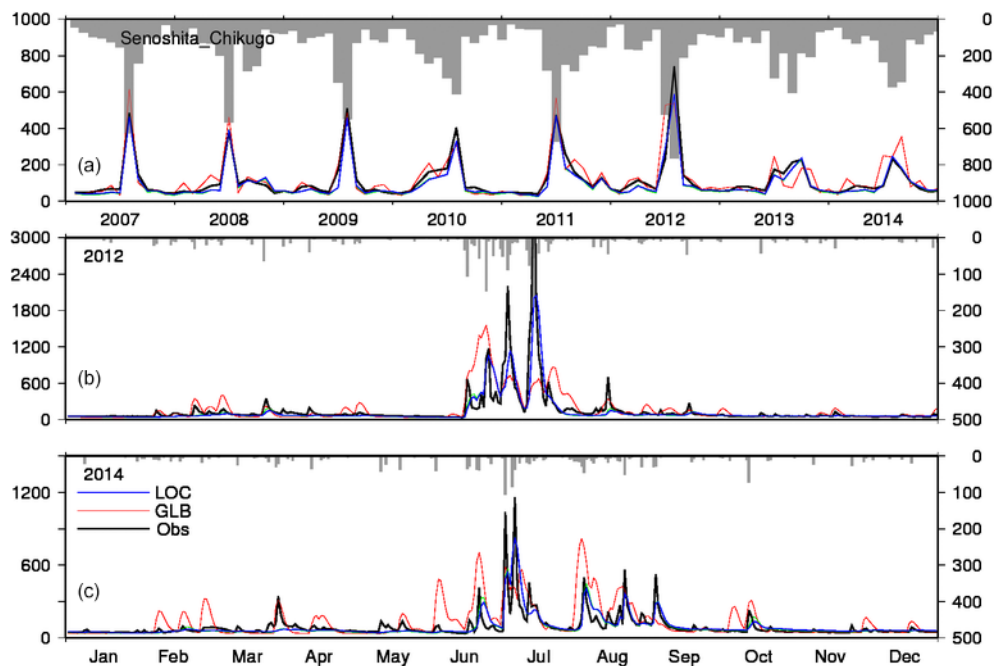


Figure 5. River discharge at Senoshita on the Chikugo River. The unit is cubic meters per second ($\text{m}^3 \text{s}^{-1}$). (a) Monthly time series of streamflow (lines) and basin-averaged precipitation in the LOC simulation (bars). (b) Daily time series of streamflow and precipitation in the wettest year of the validation period. (c) Daily time series of streamflow and precipitation in the driest year of the validation period.

levels in late June and a decrease after September. The former trend reflects precipitation during the rainy season, and the latter tendency represents permanent drainage around 30 d after flowering. In reality, when rainfall continues during the rainy season, the amount of water withdrawn is greatly restricted, but in H08, water abstraction continues unless there is a considerable amount of rainfall. Note that the rate of decrease is location dependent. For example, irrigation project C (Fig. S3) has no clear decrease period, and the simulation agreed rather well with observations at that site.

Table 7 shows the monthly NSE for the irrigation water requirements of seven irrigation projects. In general, LOC performed well, except for projects A (Fig. 6) and F. Excluding those two projects, LOC exceeded NSE values of 0.6 and, thus, substantially outperformed GLB, mainly due to the timing of irrigation. The low NSE values in A and F are due to the overestimation of the water requirement. The reasons for such an overestimation have not been fully explored and may be attributed to various possible factors, including the difference between the land use data period (1995) and simulation period (2007–2014) and region-specific irrigation practices.

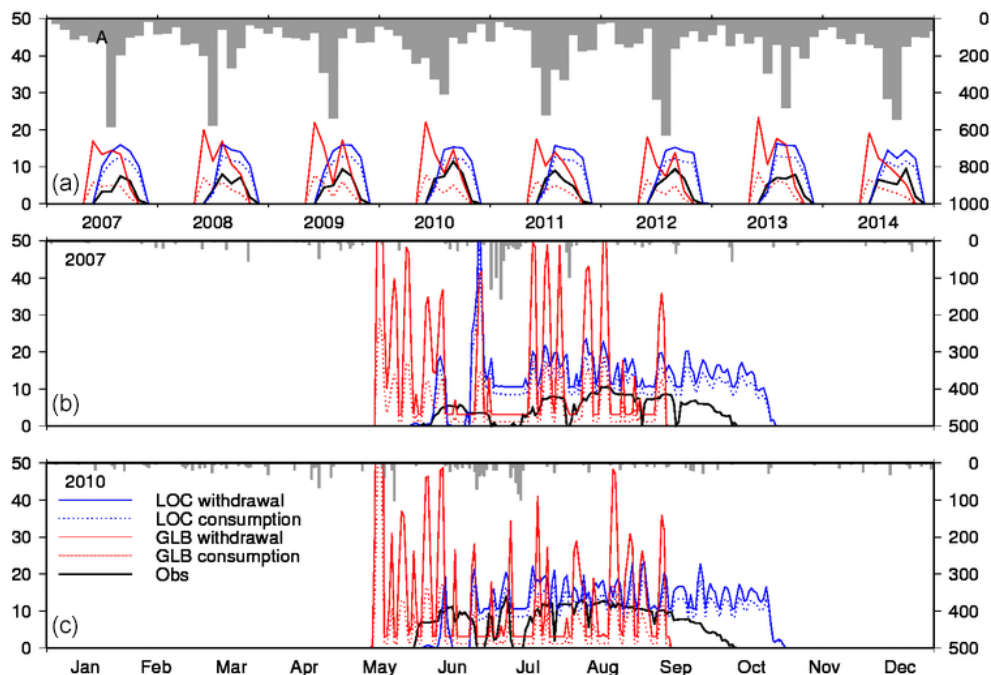


Figure 6. Irrigation water requirement at irrigation project A. (a) Monthly time series of irrigation water withdrawal (lines) and basin-averaged precipitation from the LOC simulation (bars). Solid and broken lines indicate results including and excluding irrigation efficiency, respectively. (b) Daily time series of irrigation water and precipitation in the wettest year during the validation period. (c) Daily time series of irrigation water and precipitation in the driest year during the validation period.

Table 6. Nash–Sutcliffe efficiency of daily river discharge simulations.

River	GLB	LOC
Chikugo	0.33	0.68
Oyodo	0.35	0.65
Kuma	0.37	0.73
Gokase	0.20	0.77
Sendai	0.22	0.82
Ono	0.05	0.63
Midorikawa	0.02	0.73
Onga	0.36	0.71
Kikuchi	0.20	0.71

To investigate the influence of settings, a systematic sensitivity simulation for irrigation requirement was conducted (Appendix D).

4.1.3 Reservoir operation

Figure 7 shows the results for reservoir operation at the Shimouke Dam on the Chikugo River (results for the other five dams are shown in Fig. S4). First, the monthly inflow of LOC agrees well with the observations but shows a tendency toward underestimation of the peaks, which is most apparent in 2009, 2010, 2011, 2012, and 2013. The results of GLB also agree fairly well with observations, but the tendency to-

Table 7. Monthly NSE of the irrigation requirement.

Project	GLB	LOC
A	-3.24	-1.39
B	0.13	0.66
C	-0.92	0.87
D	-0.56	0.81
E	0.32	0.64
F	-16.4	-9.54
G	0.17	0.87

ward underestimation is more prevalent, including during the dry period.

The monthly release estimates of LOC agree moderately well with observations in terms of the arrival of peaks and seasonal variations, while the estimates of GLB do not. In general, GLB tends to overestimate release in winter (October to March; apparent in 2010–2012), leading to frequent depletion (particularly in the winters of 2007, 2009, and 2013). This overestimation is due to the original algorithm of the reservoir operation submodel of H08, which was designed to release water constantly throughout the year at the rate of mean annual inflow (see Sect. 3.1.3). As numerous previous applications have demonstrated, the algorithm works well for the largest reservoirs in the world, in which total storage capacity is greater than or comparable to mean an-

nual inflow (Hanasaki et al., 2006; Masaki et al., 2017; Shin et al., 2019). However, in this reservoir, the storage capacity is only 14 % (5 %–9 % for the remaining reservoirs assessed here) of the mean annual inflow at the dam and thus is easily depleted during dry periods and overflows in wet periods. The algorithm uses several functions to avoid frequent depletion and overflow events (see Hanasaki et al., 2006), but they are not applicable to this case because the storage capacity is too small to buffer strong temporal variations in inflow.

LOC and GLB contrast sharply in the performance of their monthly storage simulations. The LOC simulation matched the observed amplitude and temporal variations in storage, while GLB results differed markedly; for example, they included extended periods of depletion (e.g., the winters of 2008, 2010, and 2012). As discussed in the previous paragraphs, the hydrographs for inflow and release generally match well. Such a run-of-the-river operation is often used for relatively small reservoirs located in rivers with high streamflow. To add the maximum possible flow control to the run-of-the-river operation, incorporation of the upper and lower storage curves (Fig. 2) is beneficial. The seasonal variations in release (Fig. 2) also played an important role in stabilizing storage (i.e., not following the upper or lower curve) and release (i.e., not falling below the intended release level) by reducing the gap between inflow and release.

Table 8 shows NSE values for six reservoirs. In general, the performance of LOC in terms of release and inflow is good (i.e., $NSE > 0.5$), except for the Iwase Dam. The inflow estimation of GLB is also good but has a lower NSE than LOC for all dams. The NSE of release is substantially lower for GLB than for LOC, mainly due to the frequent occurrence of storage depletion, which leads to zero release (Figs. 7 and S4). The NSE for storage is negative in all cases, but the values are less negative for LOC than for GLB. The difference in performance, as shown in Figs. 7 and S4, is associated with the reproducibility of the temporal variations in the storage, as discussed in the previous paragraph. Similar to irrigation water requirement, to investigate the influence of settings, a systematic sensitivity simulation for reservoir operation was conducted (Appendix E).

4.2 Water availability and use balance

4.2.1 Water sustainability index

The results presented thus far indicate that the simulation using localized data and model parameters (LOC) exhibited satisfactory performance for the estimation of streamflow in major river basins, irrigation water requirements of major projects, and the operation of major dams. Here, we assess whether water availability and use are balanced. The background for this assessment is that sufficient water is generally available on Kyushu island, except for a few locations and events, and therefore, we expect neither a large spatial extent nor a long duration of water scarcity in the study do-

main. We quantified water balance by calculating the water sustainability index (WSI), as defined in Eq. (1).

$$WSI = \frac{\sum (Riv_{DOY} + Aque_{DOY} + RGW_{DOY})}{\sum Req_{DOY}}, \quad (1)$$

where DOY represents day of year, and Σ indicates the integration of daily simulation results. Req is the total water requirement of three sectors. Riv, Aque, and RGW are daily water abstraction levels from river, aqueduct, and renewable groundwater sources, respectively. As described in Sect. 3.1.1, H08 assigns water requirements of the three sectors to five water sources. Among these sources, WSI excludes water abstraction from unspecified surface water and nonrenewable groundwater, as they indicate overuse and non-sustainable water withdrawal. WSI ranges between 0 (scarcity) and 1 (sufficiency). WSI was first introduced and used by Hanasaki et al. (2008b) and has been applied and modified in numerous studies. Its strengths and limitations relative to other indicators were summarized by Hanasaki et al. (2018a).

The distribution of mean (2007–2014) WSI is shown in Fig. 8. The results of LOC-I1 (localized model with implicit aqueducts transferring water only 1 grid cell ahead within the same basin) are shown in Fig. 8a. Under this condition, a substantial number of grid cells indicate low to severe water scarcity, including those very close to major rivers (e.g., the lower Chikugo River east of Saga city). Next, the results of LOC-I5 (same as LOC-I1 but with a transfer of up to five grid cells ahead) are shown in Fig. 8b. Although a substantial number of water insufficient grid cells remained, water scarcity was attenuated across the entire domain because water could be transferred a maximum of five grid cells ahead, thereby connecting grid cells with large water requirements to those with large water availability (e.g., northeast of Fukuoka). Then, the results of LOC-I50 (same as LOC-I5 but allowing water transfer outside of basins with small catchment areas) are shown in Fig. 8c. Because water demand is concentrated along the seashore, interbasin water transfer reduced water scarcity in coastal areas dramatically (e.g., southwest of Kumamoto). Finally, the results of LOC-I50E (same as LOC-I50 but including explicit aqueducts) are shown in Fig. 8d. Under this condition, water scarcity was further attenuated (e.g., the lower reach of the Chikugo River near Saga city). Places with exceptionally low WSI are discussed in the next subsection.

The numbers of grid cells with WSI values below 0.99, 0.80, and 0.50 are shown in Table 9. As the total number of grid cells in the study domain is 13 105, approximately 6 %–8 % of grid cells are categorized as experiencing at least low water scarcity ($WSI < 0.99$). The introduction of numerous aqueducts efficiently decreases the number of grid cells with water scarcity, and the effects are stronger for more severe scarcity levels. The number of grid cells is reduced from 1110 (LOC-I1) to 746 (LOC-I50E) for $WSI < 0.99$ and from 28 to 1 for $WSI < 0.5$ with the addition of aqueducts.

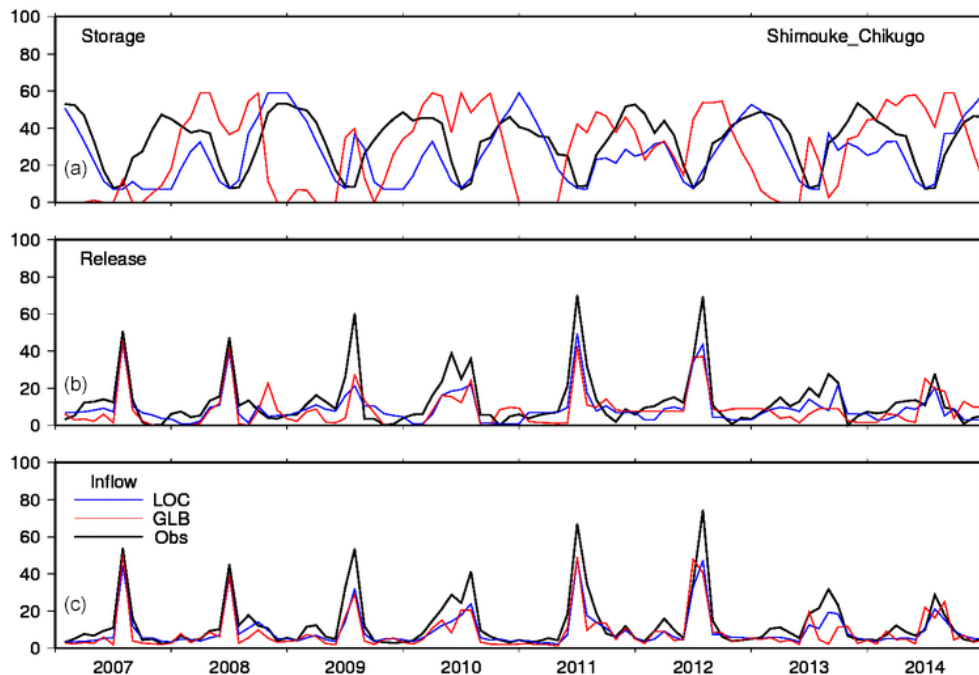


Figure 7. Reservoir operation at the Shimouke Dam on the Chikugo River. (a) Monthly time series of water storage ($10^6 \text{ m}^3 \text{ yr}^{-1}$). (b) Monthly time series of release ($\text{m}^3 \text{ yr}^{-1}$). (c) Monthly time series of inflow ($\text{m}^3 \text{ yr}^{-1}$).

Table 8. NSE values for monthly storage, release, and inflow.

	GLB			LOC		
	Storage	Release	Inflow	Storage	Release	Inflow
Shimouke	-3.01	0.48	0.61	-0.08	0.68	0.77
Midorikawa	-52.0	-0.02	0.20	-7.51	0.87	0.85
Tsuruda	-12.3	0.32	0.61	-3.43	0.90	0.92
Ichifusa Dam	-11.6	0.47	0.72	-0.08	0.86	0.88
Kitagawa	-3.58	0.34	0.56	-0.62	0.59	0.68
Iwase	-26.7	-1.20	-0.80	-0.95	-0.77	-0.85

Table 9. Numbers of grid cells below the WSI thresholds.

	WSI < 0.5	WSI < 0.8	WSI < 0.99
LOC-I1	28	253	1110
LOC-I5	16	191	941
LOC-I50	5	88	795
LOC-I50E	1	54	746

4.2.2 Locations with low WSI

We investigated locations with medium water scarcity ($\text{WSI} < 0.8$) in the LOC-I50E simulation. Such grid cells are concentrated in four dominant regions, namely the Saga plain (near Saga city), the Shiroishi plain (southwest of Saga city, connected to the Saga plain), the Kitano plain (southeast of Fukuoka city), and Usa city (northwest of Ōita city;

see Fig. S5). We collected information about these regions with the goal of clarifying the reason for low WSI. The information sources used are listed in Table S7 but most are available only in Japanese.

The Saga plain contains vast areas of irrigated cropland mainly supplied from the Kasegawa River (catchment area 368 km^2), which flows near the center of Saga city. The irrigation system in that area consists of the Kitagawa Dam (a single-purpose dam supplying irrigation water to the Saga plain), the Kawakami Weir, and a dense network of irrigation canals. The LOC-I50E simulation includes the river, weir, and canals (i.e., explicit aqueducts) but lacks the Kitagawa Dam because its storage capacity of $22.25 \times 10^6 \text{ m}^3$ is below the threshold of $40 \times 10^6 \text{ m}^3$ used in this study. Thus, the low WSI estimate is at least partially attributable to the underestimation of water availability (i.e., exclusion of the dam limits water supply in the dry period).

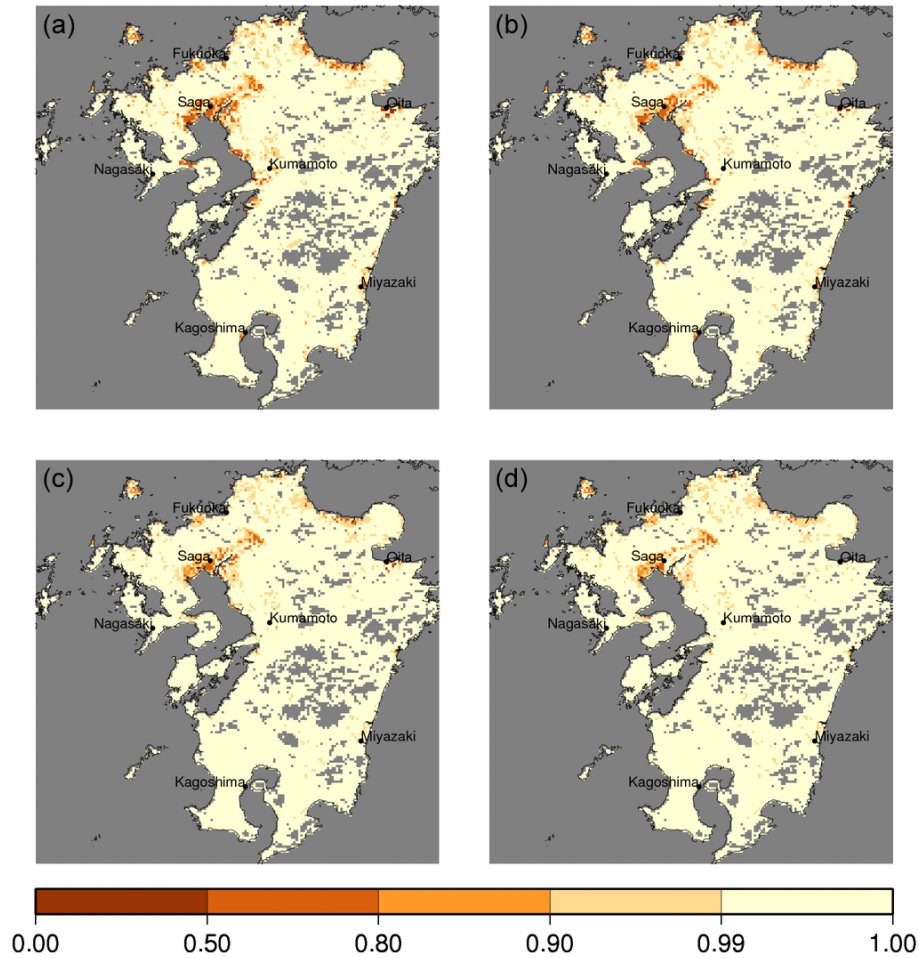


Figure 8. Water sustainability index. (a) LOC-I1 (localized model with implicit aqueducts transferring water to one adjacent grid cell), (b) LOC-I5 (localized model with implicit aqueducts transferring water to a maximum of five surrounding grid cells), (c) LOC-I5O (localized model with implicit aqueducts transferring water to a maximum of five grid cells, including cells outside the basin), and (d) LOC-I5OE (localized model with implicit aqueducts transferring water to a maximum of five grid cells, including cells outside the basin as well as explicit aqueducts). Symbols show the centers of prefecture capital cities. For visibility, only the mean annual withdrawal $>0.03 \text{ m}^3 \text{ s}^{-1}$ is shown.

Shiroishi plain is located to the southwest of Saga city, along Ariake Sea. A considerable portion of the plain is reclaimed land that is distant from major rivers. Historically, the area has been irrigated using groundwater pumping. After completion of the Kasegawa Dam in 2012, which is located below the Kitagawa Dam, a new surface water irrigation project was initiated to divert water from the Kasegawa River to this area, but that project was not included in the present study because it was operational only during the last 3 years of the simulation period (2012–2014). Because no detailed data on the spatial distribution of irrigation water sources were available, we used global data at 5×5 arcmin resolution (Siebert et al., 2010), which indicated that only approximately 7% of the area is appropriate for groundwater irrigation.

The Kitano plain is located southeast of Fukuoka (and northeast of Saga) on the right bank of the middle reach of the Chikugo River. The project in that area is the Ryochiku Heiya Irrigation Project, which is supplied mainly by two tributaries of the Chikugo River, namely the Koishwaragawa River (catchment area of 85.9 km^2) and the Satagawa River (catchment area, 73.6 km^2). Each river has one major dam, namely the Egawa Dam ($25.33 \times 10^6 \text{ m}^3$) and the Terauchi Dam ($18 \times 10^6 \text{ m}^3$), respectively. Similar to the Saga plain example, these two dams were excluded from this study, and thus, the underestimation is at least partially attributable to the lack of these dams in the simulation.

Usa city is located along the downstream portion of the Yakkan River (catchment area, 430 km^2) facing the western extreme of the Seto Inland Sea. Because this area is surrounded by mountains, the basin receives less precip-

itation than other areas (the mean annual precipitation is 1400 mm yr^{-1}). Dams on the upstream portion of the Yakkan River and the presence of hundreds of irrigation ponds may play vital roles in the low WSI of this area.

4.3 Uncertainty

In this study, we validated the simulated streamflow, irrigation water withdrawal, and reservoir operation for the downstream gauging station of the nine largest rivers, seven national irrigation projects, and six reservoirs on Kyushu island. The results were reasonably good, indicating that the overall hydrological processes and human water use and management were properly simulated at the scales used for validation. Nonetheless, the water supply and demand balance were not fully closed for all grid cells, indicating that further efforts are needed.

4.3.1 Infrastructure

The discussion in the previous subsection indicates that cases of possible water scarcity occur in river basins, including reservoirs smaller than the threshold size (i.e., $<40 \times 10^6 \text{ m}^3$). To incorporate the dams we noted above, the threshold for reservoir storage capacity should be lowered to $18 \times 10^6 \text{ m}^3$ for the study domain. The number of reservoirs meeting this threshold is 29, among which reservoir operation records for 24 are available. Additionally, the major weirs and aqueducts should be georeferenced into the digital river map. Moreover, no severe and extensive droughts were recorded in the study period. During such events, the role of water management infrastructure would be prominent.

4.3.2 Groundwater

In this study, we fixed the surface water and groundwater usage rate to a uniform value across a vast study domain, as the spatial distribution of data was unavailable. As discussed for Shiroishi plain, some regions use groundwater intensively. Another apparent exception to the uniform value is Kumamoto city, where 100 % of the municipal water is supplied by groundwater (Kumamoto City, 2015). Aside from usage, the recharge and flow of groundwater may be additional sources of uncertainty. For example, Mount Aso, which is located at the center of Kyushu island, is an active volcano. The soil in the surrounding area is highly permeable and forms abundant groundwater. The lack of hydrogeological detail in this model is another source of uncertainty.

4.3.3 Municipal water systems

In this study, we have introduced the implicit and explicit aqueducts which allow water withdrawal from surrounding grid cells where water resources are abundant. This is particularly important for urban areas where municipal and industrial water is highly concentrated. Although improved com-

pared to earlier approaches (e.g., Wada et al., 2016) which assumed water withdrawal and use occurred in a single grid cell, there is still room for progress. Kyushu island contains seven cities, with populations greater than 400 000, and many other settlements. The urban areas of such cities cover dozens of grid cells, which are served by municipal water supply and sewage systems. For urban areas, water is withdrawn at a limited number of inlets to treatment plants and released at outlets from sewage treatment plants. In contrast, H08 allows for water abstraction and drainage from every grid cell, as it was originally developed for a spatial resolution of 30 arcmin, at which the effects of urban water systems become negligible. Thus, water scarcity may be underestimated in major cities in this simulation, which allows for usage of water from one grid cell upstream, or an intensive cascade of drainage among neighboring cells, but completely ignores the presence of municipal water systems. This problem will be largely solved by including waterwork facilities (i.e., water treatment plants, water and sewer pipe networks, and wastewater treatment plants) into the model. This will make the simulation more realistic in terms of representation of the urban water scarcity problem.

4.3.4 Natural hydrological processes

While this study has mainly focused on the processes of water use and management, natural hydrological processes also need to be further improved. Snow falls only in limited mountainous areas of Kyushu island, and therefore, the performance of snow process estimation was not evaluated in this study. Groundwater is expressed in highly conceptual way in H08 (treated as a hypothetical tank), which hampers the validation of groundwater simulation. As for the lateral flows of subsurface water, Ji et al. (2017) reported that they matter to the distribution of soil moisture and evapotranspiration at the spatial resolution of 1000 m and finer. The inclusion of the process is crucial, particularly in the regions where groundwater is the major water source. As such, the dominant hydrological processes differ region by region. Further application and investigation of the model under various environment is indispensable to fully realizing globally applicable hyper-resolution modeling.

4.4 Lessons for hyper-resolution global hydrological modeling

This study presents a method of validation, localization, and utilization for water resource assessment based on hyper-resolution global hydrological data. The study domain is $37\,500 \text{ km}^2$, which is approximately 1/10 of the land area of Japan ($378\,000 \text{ km}^2$) and 1/3600 of the total land on Earth ($135 \times 10^6 \text{ km}^2$, excluding Antarctica). Eventually, the simulation and validation domains should be extended by 3 orders of magnitude. In this subsection, we discuss how such global extension may be realized.

4.4.1 Validation

River discharge is the easiest factor to validate, but the process has two prerequisites. First, a reliable flow direction map, which reflects the actual shapes of basins and catchment areas of major river gauging points, is needed. Second, a standardized river discharge publication system is required, and must be well designed for (semi-) automatic data retrieval. The water information system used in this study is a good example of such a publication platform but is optimized for manual data retrieval through mouse operation. Also it is only available in Japanese, hindering data retrieval by non-Japanese-speaking users. Such detailed data provisioning systems are commonly available for developed countries but not for other regions. Although efforts have been made to collect historical river discharge records for a considerable number of river basins (van Dijk et al., 2013; Beck et al., 2013), further database development is needed for global hydrological research.

The validation of reservoir operations is more challenging than validation of river discharge. First, reservoir operation records are far less frequently published. This difference is due in part to the fact that reservoirs are operated by multiple agencies. For example, of the 29 reservoirs on Kyushu (i.e., $>18 \times 10^6 \text{ m}^3$), eight are operated by the Ministry of Land Infrastructure Transport and Tourism (central government), four by the Japan Water Agency (central governmental agency), 13 by prefectures, one by the Ministry of Agriculture Forestry and Fisheries (central government), and three by Kyushu Electric Power Company (private company). Differences in the volume of publicly accessible data exist among these organizations. Satellite-based estimations of reservoir operation is a promising technology (Busker et al., 2019) but may be difficult to apply to Kyushu due to its small lake area and frequent cloud coverage.

4.4.2 Data localization

Elevation and river topography data are available globally at 3 arcsec or 90 m resolution (Yamazaki et al., 2017, 2019). A central data issue is the upscaling of such fine-scale data to coarser (e.g., 3 to 30 arcsec) resolution, which is not a trivial problem (Yamazaki et al., 2009). In addition, proper transfer of gauging station and infrastructure (e.g., reservoirs, weirs, and canal networks) data is essential. Collection and georeferencing of data for aqueducts and weirs is a challenging issue. Although previous attempts to estimate the water transfer of large cities (McDonald et al., 2014) and mega-projects (Shumilova et al., 2018) have been reported, far more extensive efforts are needed to achieve global coverage, including small projects (neither of the previously cited works covered any of the aqueducts included in this study).

Most global agricultural data are available at 5 arcmin resolution (Ramankutty et al., 2008; Monfreda et al., 2008; Siebert et al., 2005, 2010). As noted above, 5 arcmin res-

olution is too coarse for use with 1 arcmin or finer resolution. Because land use and crop type significantly affect water demand, their areal information should be obtained from a national agricultural census. Digitizing and georeferencing census results is crucially important (Kohyama et al., 2003). Some factors, including the irrigation water withdrawal, fraction of groundwater use, irrigation efficiency, and crop calendar, are hard to obtain. Systematic collection of data on such everyday agricultural practices is crucial.

Perhaps the most important data type in terms of simulation performance is meteorological data. The overall performance of this simulation depends on good meteorological data, especially high-quality precipitation data. Most global meteorological data currently available have spatial resolution of 30 arcmin (Weedon et al., 2014; Cucchi et al., 2020). Recent efforts have made some of meteorological data available at 15 arcmin resolution (Beck et al., 2017; Hersbach et al., 2020; Yatagai et al., 2012), but a gap in the spatial resolution remains. A community effort with regard to data standardization and sharing is essential for future progress.

4.4.3 Model localization

In this study, the model was localized in four aspects, namely hydrological parameters, irrigation parameters, reservoir operation settings, and implicit canal estimation configuration. First, hydrological parameter optimization can be more systematically applied. Yoshida et al. (2021) demonstrated the semi-automatic parameter optimization of H08 based on 777 river gauges globally, which is a promising technique for hyper-resolution global application. For irrigation and reservoir parameter settings, the applicability of the methodology devised in this study to other regions remains unknown. Further modification or improvement will likely be needed for application to other parts of Japan and the world, as hydrometeorological conditions differ significantly among regions. Identification of key formulas and parameters to represent various water use practices will continue. Rigorous databasing of large-scale aqueducts and further algorithm validation would make the implicit canal inference process applicable to a broad range of regions. Last, the validity of implicit canal estimation was demonstrated only indirectly in this study. The results indicate great improvement of the balance between water supply and demand in the study domain, with realistic results for Kyushu island, but direct validation against a more detailed database of weirs and canals is required for generalizing the origins and destinations of water diversion networks in Japan.

4.4.4 Assessment

High-resolution water assessment will provide novel insights into issues related to water resources. For example, the water scarcity distribution shown in Fig. 8 is a reminder of how sensitive water availability is to climatic and geographic con-

ditions. Water scarcity may occur around tributaries of major rivers (e.g., the Kitano plain), although such areas have been largely overlooked in low-resolution modeling efforts. The present study also highlights the importance of aqueducts and reservoirs, which play crucial roles in balancing water demand and supply. Ignoring water infrastructure may result in misleading water resource assessment results.

5 Conclusions

In this study, we applied the global hydrological model H08 to Kyushu island, at a spatial resolution of 1 arcmin, to address three research questions. First, in terms of the reproducibility of the default H08 model and simulation settings, the detailed validation results indicate highly negative values, suggesting that a simple increase in the spatial resolution of global simulation does not lead to reliable results at the local scale. The results highlight the importance of rigorous validation of the most important variables and locations. Second, the process of model localization was demonstrated as promising and effective. Localization of the data and model improve the performance to a satisfactory level (e.g., daily streamflow NSE > 0.5). The prerequisites for localization are good availability, accessibility, and trustworthiness of hydrometeorological data, as well as abundant local water resource information, including historical data. Third, as a benefit of hyper-resolution simulation, we confirmed that the model could support city- or irrigation district-wide assessment. The results highlighted the importance of water management facilities (reservoirs, weirs, and canals) and water use information (groundwater usage and irrigation efficiency). We identified various factors that sustain local water use through examination of a spatially detailed simulation that had been largely overlooked in standard global simulation studies, which are typically at 30 arcmin resolution.

This study contributes to hydrological science in three ways. First, this is the first study to provide an example application of a global water resources model to 1 arcmin spatial resolution. Although the study domain was rather limited ($3^\circ \times 3^\circ$), it opens the door to application of the model to hyper-resolution global hydrology. Second, this is the first study to provide a detailed comparison of global and localized simulations using exactly the same source code. We demonstrated that global models can be used as regional hydrological models with reasonable effort. Third, based on our findings, we identified gaps in the existing process and proposed steps toward hyper-resolution global water resources modeling.

For practical climate change adaptation planning and water resource development, local human water use and management are non-negligible problems that can be addressed with sophisticated hyper-resolution global modeling. The detailed information obtained from this study can be utilized to support the recent trend toward identifying environmen-

tal impacts of corporate activities in a meaningful manner (e.g., CDP water security; <https://www.cdp.net/en/>, last access: 11 April 2022).

Appendix A: Conversion of sunshine duration into downward shortwave radiation

We converted sunshine duration (h; s_d) into downward shortwave radiation (W m^{-2}) using the following equation from Kondo (1994).

$$\frac{s_d}{s_{d0}} = 0.244 + 0.511 \left(\frac{N}{N_0} \right), \quad (\text{A1})$$

where s_{d0} is solar irradiance at the top of the atmosphere (W m^{-2}), N is sunshine duration (h), and N_0 is maximum possible sunshine duration (h).

Appendix B: Estimation of downward longwave radiation

We estimated downward longwave radiation (W m^{-2} ; L_d^\downarrow) using the following equation from Kondo (1994).

$$L_d^\downarrow = \sigma T^4 \left[1 - \left(1 - \frac{L_{\text{df}}^\downarrow}{\sigma T^4} \right) C \right] \quad (\text{B1})$$

$$L_{\text{df}}^\downarrow = \left(0.74 + 0.19 \log_{10} w_{\text{TOP}} + 0.07 (\log_{10} w_{\text{TOP}})^2 \right) \sigma T^4 \quad (\text{B2})$$

$$C = 0.826 \left(\frac{N}{N_0} \right)^3 - 1.234 \left(\frac{N}{N_0} \right)^2 + 1.135 \left(\frac{N}{N_0} \right) + 0.298, \quad (\text{B3})$$

where σ is the Stefan–Boltzmann constant, T is air temperature (K), L_{df}^\downarrow is clear-sky downward longwave radiation (W m^{-2}), and w_{TOP} is effective vapor volume (cm).

Appendix C: Sensitivity simulation on river discharge

We have decomposed the differences between GLB and LOC simulations into the following three factors: (A) calibration, (B) local meteorological observation, and (C) high spatial resolution of data. The combination of factors is shown in Table C1.

YYY and NNN are identical to the LOC and the GLB simulations, respectively. YYY and NYY use the high-resolution daily local meteorological observation (AMeDAS). YNN and NNN use the global meteorological data (WFDEI; Weedon et al. 2014). YYN and NYN use the low-resolution AMeDAS, which was prepared as follows: we aggregated the AMeDAS data for 30×30 grid cells in 1 arcmin and converted them into one large grid cell in 30 arcmin (identical to the data resolution of WFDEI) then linearly interpolated

the data again into 30×30 grid cells in 1 arcmin. In this way, only the spatial resolution of AMeDAS was decayed. YNY and NNY are not available, since they require global meteorological data (reanalysis) as fine as 1 arcmin spatial resolution, which do not exist as of yet.

The results are shown in Fig. C1. In general, the calibration increases the NSE for many cases if other conditions are identical (21 out of 27), but the effect (the change in NSE) is limited. Exceptions are seen, for example, in Stations 1, 6, and 8, where NYY (without calibration) performs slightly better than YYY (with calibration). This is considered that due to possible overfitting during the calibration period. Next, high spatial resolution increases the NSE for most of the cases (16 out of 18) but again the effect is limited. Exceptions are seen in Stations 2 and 5, where NYN (low resolution) outperforms NYY (high resolution). Finally, local meteorological data significantly increases the NSE for all the cases (18 out of 18 by the median of 0.43).

The results of sensitivity test clearly indicate that the usage of local meteorological observation is the key factor in the simulation performance. As mentioned earlier, the timing and magnitude of submonthly weather events in the global meteorological data (WFDEI) are based on reanalysis which are not always successful in reproducing the timing and the location where weather events occurred.

Table C1. Sensitivity simulation. The simulation names and the combinations of factors are given.

Simulation	YYY	YYN	YNN	NYY	NYN	NNN
Calibration	Yes	Yes	Yes	No	No	No
Local meteorological observation	Yes	Yes	No	Yes	Yes	No
High resolution	Yes	No	No	Yes	No	No

The reproducibility of reanalysis is being improved generation by generation. By using the latest global meteorological data based on the latest generation of reanalysis, the GLB simulation is expected to perform better (e.g., the WFDE5, Cucchi et al., 2020, which uses the ERA5 reanalysis; Hersbach et al., 2020).

Appendix D: Sensitivity simulation on irrigation requirement

We have decomposed the differences between GLB and LOC simulations into the following three factors: adoption of (A) local crop calendar, (B) local cropping practices, and (C) local hydrometeorological conditions. The combination of factors is shown in Table D1.

The sensitivity simulations SI1, SI2, SI3 were identical to LOC, except for the aforementioned three factors. SI1

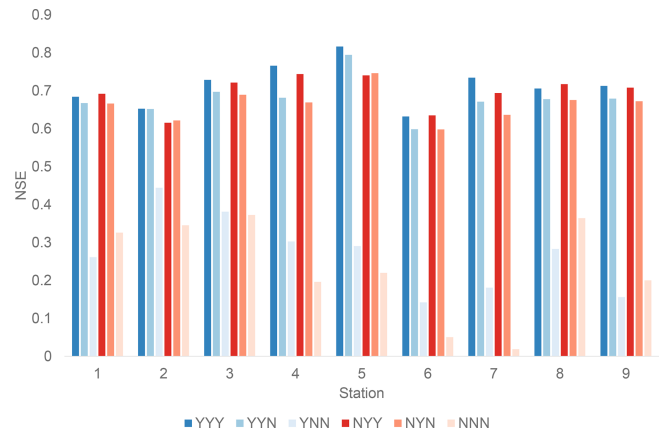


Figure C1. The results of sensitivity analysis on river discharge. See Table C1 for simulation runs. YYY and NNN correspond to the GLB and LOC simulations, respectively.

replaced the adjusted crop calendar for rice with the originally simulated one (Sect. 3.2.3). SI2 is same as SI1 but additionally replaced the localized settings of the land use (Sect. 3.2.3, Fig. 4) and the irrigation efficiency parameter (Sect. 3.2.3) with those of GLB. Here, crop calendar, land use, and irrigation efficiency are all essential in estimating irrigation water requirement but virtually solely available from governmental reports and, hence, hard to obtain globally. We singled out the crop calendar (i.e., separated SI1 and SI2) because it would be available in the future globally since some concrete methods have been proposed by utilizing the latest satellite remote sensing techniques (Kotsuki and Tanaka, 2015). SI3 is same as SI2 but additionally replaced the local meteorological data with the global ones and the calibrated hydrological parameters with the default ones (Sect. 3.1.2 and 3.2.1).

The results are shown in Fig. D1. In general, the NSE scores for SI1, SI2, and SI3 are deteriorated in this order and approaching those for GLB. The apparent exception is the influence of local cropping practices (i.e., SI2). The irrigation efficiency of GLB is set at 0.35 uniformly, while LOC is at 0.45–0.8. The adoption of low efficiency inflates irrigation water requirement which drastically decreases the NSE score. The effect is canceled out when the global hydrometeorological conditions are applied, which suppresses the total irrigation water requirement (Sect. 4.1.2).

In contrast to the sensitivity test for discharge shown in Appendix C, the influence of adopting local meteorological condition looks marginal. This is, however, largely due to the considerable drop in the NSE score caused by other factors. This sensitivity simulation highlights the importance of reliable local cropping practices. They can alter the shape, the phase, and the magnitude of simulation time series and are, hence, highly influential in the results and performances.

Table D1. Sensitivity simulation on irrigation requirement.

Simulation	LOC	SI1	SI2	SI3	GLB
Local crop calendar	Yes	No	No	No	No
Local cropping practices	Yes	Yes	No	No	No
Local hydrometeorological conditions	Yes	Yes	Yes	No	No
Model	LOC	LOC	LOC	LOC	GLB

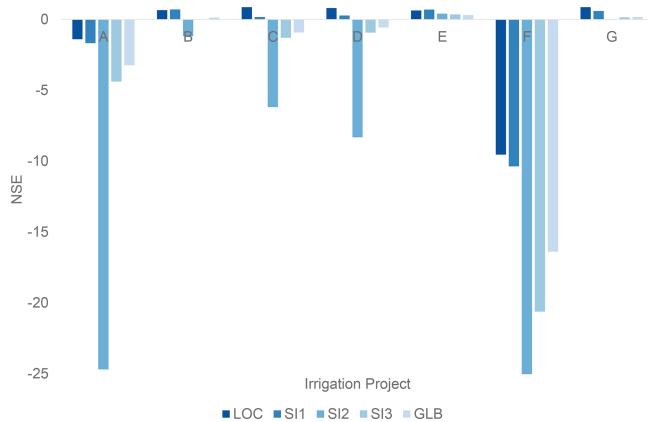


Figure D1. The results of sensitivity analysis. See Table D1 for simulation runs. The NSE for irrigation project F (SI2) is -98.4 .

Appendix E: Sensitivity simulation on reservoir operation

We have decomposed the differences between GLB and LOC simulations into the following three factors: adoption of (A) upper and lower storage rule curves (Fig. 2a), (B) release curve (Fig. 2b), and (C) local hydrometeorological conditions. The combination of factors is shown in Table E1.

The sensitivity simulations SD1, SD2, and SD3 were identical to LOC except for the three factors. SD1 removed the setting of upper and lower storage curves (Sect. 3.1.3, Fig. 2). This setting allows the storage to fluctuate, at any time, between being completely depleted and completely full. SD2 is same as SD1 but, additionally, removed the release curve. This setting fixes the release throughout a year at the mean annual inflow (see Hanasaki et al., 2006, for the complete formulations). Although these curves are essential in the actual reservoir operation, it is hard to obtain globally. The advances in satellite global reservoir monitoring would offer the opportunity to estimate the upper and lower storage curves for major reservoirs (Busker et al., 2019). Hence, we considered that the chance of earning the storage curves (SD1) is more likely than the release one (SD2). SD3 is same

as SD2 but additionally replaced the local meteorological data with the global data and the calibrated hydrological parameters with the default parameters (Sect. 3.1.2 and 3.2.1).

Table E1. Sensitivity simulation on reservoir operation.

Simulation	LOC	SD1	SD2	SD3	GLB
Storage curves	Yes	No	No	No	No
Release curve	Yes	Yes	No	No	No
Local hydrometeorological conditions	Yes	Yes	Yes	No	No
Model	LOC	LOC	LOC	LOC	GLB

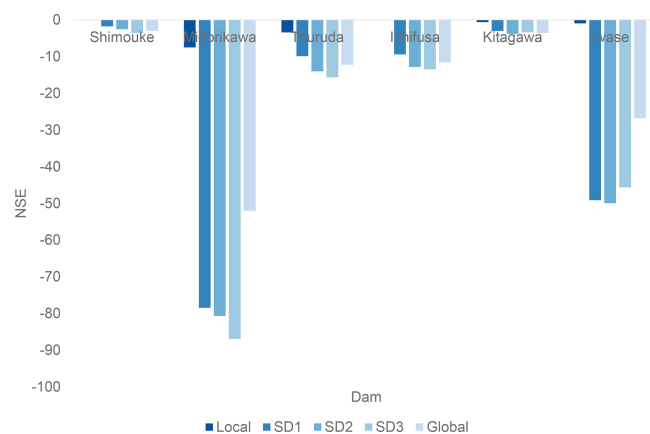


Figure E1. Sensitivity analysis for reservoir storage. See Table E1 for the simulation runs.

The results for storage are shown in Fig. E1. In general, the NSE scores for SD1, SD2, and SD3 are deteriorated in this order and approaching that of GLB. Note that SD3 and GLB do not completely agree because of other settings between LOC and GLB (e.g., water withdrawal and diversion). The removal of storage curves has the largest impact on the performance of storage simulation, which can be easily expected. The storage capacity of the dams is relatively small compared to their inflow, which typically causes strong storage variations. Once the constraints due to storage rule curves are lost, the simulated storage showed considerable variations by reflecting errors in inflow and release.

The results for release are shown in Fig. E2. Again, the NSE scores for SD1, SD2, and SD3 are deteriorated in this order and approaching that of GLB. The impacts due to the adoption of the storage curves, the release curve, and the local hydrometeorological data are not easily discernible, except in the case for the Midorikawa Dam and the Tsuruda Dam. For these two reservoirs, the adoption of local hydrometeorological data dominantly influenced the simulation performance.

Overall, specifying the key factors in the performance of reservoir operation simulation is harder than the discharge (Appendix C) and irrigation requirement (Appendix D). This is likely due to the overall low reproducibility of the reality and, in particular, the storage variation. Further fundamental improvement is needed in reservoir modeling to reproduce the operations of the past.

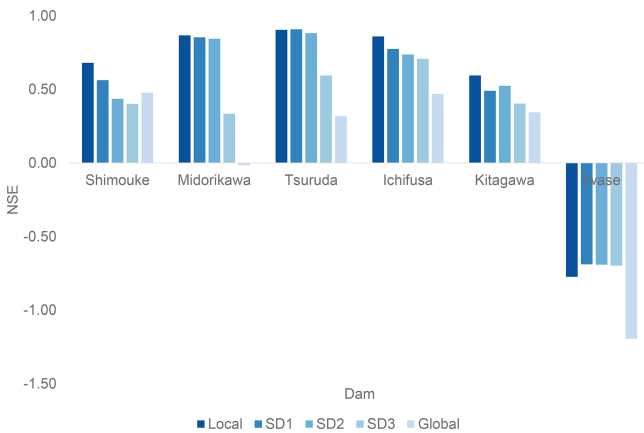


Figure E2. Sensitivity analysis for reservoir release. See Table E1 for the simulation runs.

Code and data availability. Code and data are available at <https://doi.org/10.5281/zenodo.5523280> (Hanasaki, 2021).

Supplement. The supplement related to this article is available online at: <https://doi.org/10.5194/hess-26-1953-2022-supplement>.

Author contributions. NH designed the experiments, and NH, HM, and MF carried them out. NH, HM, and MF developed the model code and performed the simulations. YH, SS, SK, and TO validated the model. NH prepared the paper, with contributions from all co-authors.

Competing interests. The contact author has declared that neither they nor their co-authors have any competing interests.

Disclaimer. Publisher's note: Copernicus Publications remains neutral with regard to jurisdictional claims in published maps and institutional affiliations.

Acknowledgements. The authors are grateful to Noemi Vergopolan, the two anonymous referees, and Luca Brocca, for providing comments on this work. This research has been supported by KAKENHI (grant nos. 16H06291, 21H05178, and 21H05002) of the Japan So-

ciety for the Promotion of Science. The authors are responsible for any errors.

Financial support. This research has been supported by the Japan Society for the Promotion of Science (KAKENHI; grant nos. 16H06291, 21H05178, and 21H05002).

Review statement. This paper was edited by Xing Yuan and reviewed by Noemi Vergopolan and two anonymous referees.

References

- Alcamo, J., Döll, P., Henrichs, T., Kaspar, F., Lehner, B., Rösch, T., and Siebert, S.: Development and testing of the WaterGAP 2 global model of water use and availability, *Hydrolog. Sci. J.*, 48, 317–337, <https://doi.org/10.1623/hysj.48.3.317.45290>, 2003a.
- Alcamo, J., Döll, P., Henrichs, T., Kaspar, F., Lehner, B., Rösch, T., and Siebert, S.: Global estimates of water withdrawals and availability under current and future “business-as-usual” conditions, *Hydrolog. Sci. J.*, 48, 339–348, 2003b.
- Arnold, J. G., Kiniry, J. R., Srinivasan, R., Williams, J. R., Haney, E. B., and Neitsch, S. L.: SWAT Input/Output Documentation Version 2012, Texas Water Resources Institute, TR-439, 654, <https://swat.tamu.edu/media/69296/swat-io-documentation-2012.pdf> (last access: 11 April 2022), 2012.
- Beck, H. E., van Dijk, A. I. J. M., Miralles, D. G., de Jeu, R. A. M., Bruijnzeel, L. A., McVicar, T. R., and Schellekens, J.: Global patterns in base flow index and recession based on streamflow observations from 3394 catchments, *Water Resour. Res.*, 49, 7843–7863, <https://doi.org/10.1002/2013WR013918>, 2013.
- Beck, H. E., van Dijk, A. I. J. M., de Roo, A., Miralles, D. G., McVicar, T. R., Schellekens, J., and Bruijnzeel, L. A.: Global-scale regionalization of hydrologic model parameters, *Water Resour. Res.*, 52, 3599–3622, <https://doi.org/10.1002/2015wr018247>, 2016.
- Beck, H. E., van Dijk, A. I. J. M., Levizzani, V., Schellekens, J., Miralles, D. G., Martens, B., and de Roo, A.: MSWEP: 3-hourly 0.25° global gridded precipitation (1979–2015) by merging gauge, satellite, and reanalysis data, *Hydrol. Earth Syst. Sci.*, 21, 589–615, <https://doi.org/10.5194/hess-21-589-2017>, 2017.
- Becker, J. J., Sandwell, D. T., Smith, W. H. F., Braud, J., Binder, B., Depner, J., Fabre, D., Factor, J., Ingalls, S., Kim, S. H., Ladner, R., Marks, K., Nelson, S., Pharaoh, A., Trimmer, R., Von Rosenberg, J., Wallace, G., and Weatherall, P.: Global Bathymetry and Elevation Data at 30 Arc Seconds Resolution: SRTM30_PLUS, *Mar. Geod.*, 32, 355–371, <https://doi.org/10.1080/01490410903297766>, 2009.
- Burek, P., Satoh, Y., Kahil, T., Tang, T., Greve, P., Smilovic, M., Guillaumot, L., Zhao, F., and Wada, Y.: Development of the Community Water Model (CWatM v1.04) – a high-resolution hydrological model for global and regional assessment of integrated water resources management, *Geosci. Model Dev.*, 13, 3267–3298, <https://doi.org/10.5194/gmd-13-3267-2020>, 2020.
- Busker, T., de Roo, A., Gelati, E., Schwatke, C., Adamovic, M., Bisselink, B., Pekel, J.-F., and Cottam, A.: A global lake and reservoir volume analysis using a surface water dataset

- and satellite altimetry, *Hydrol. Earth Syst. Sci.*, 23, 669–690, <https://doi.org/10.5194/hess-23-669-2019>, 2019.
- Cucchi, M., Weedon, G. P., Amici, A., Bellouin, N., Lange, S., Müller Schmied, H., Hersbach, H., and Buontempo, C.: WFDE5: bias-adjusted ERA5 reanalysis data for impact studies, *Earth Syst. Sci. Data*, 12, 2097–2120, <https://doi.org/10.5194/essd-12-2097-2020>, 2020.
- Dalin, C., Wada, Y., Kastner, T., and Puma, M. J.: Groundwater depletion embedded in international food trade, *Nature*, 543, 700, <https://doi.org/10.1038/nature21403>, 2017.
- Dee, D. P., Uppala, S. M., Simmons, A. J., Berrisford, P., Poli, P., Kobayashi, S., Andrae, U., Balmaseda, M. A., Balsamo, G., Bauer, P., Bechtold, P., Beljaars, A. C. M., van de Berg, L., Bidlot, J., Bormann, N., Delsol, C., Dragani, R., Fuentes, M., Geer, A. J., Haimberger, L., Healy, S. B., Hersbach, H., Hólm, E. V., Isaksen, I., Kållberg, P., Köhler, M., Matricardi, M., McNally, A. P., Monge-Sanz, B. M., Morcrette, J.-J., Park, B.-K., Peubey, C., de Rosnay, P., Tavolato, C., Thépaut, J.-N., and Vitart, F.: The ERA-Interim reanalysis: configuration and performance of the data assimilation system, *Q. J. Roy. Meteor. Soc.*, 137, 553–597, <https://doi.org/10.1002/qj.828>, 2011.
- De Roo, A. P. J., Wesseling, C. G., and Van Deursen, W. P. A.: Physically based river basin modelling within a GIS: the LISFLOOD model, *Hydrol. Process.*, 14, 1981–1992, [https://doi.org/10.1002/1099-1085\(20000815/30\)14:11/12<1981::AID-HYP49>3.0.CO;2-F](https://doi.org/10.1002/1099-1085(20000815/30)14:11/12<1981::AID-HYP49>3.0.CO;2-F), 2000.
- Döll, P. and Siebert, S.: Global modeling of irrigation water requirements, *Water Resour. Res.*, 38, 1037, <https://doi.org/10.1029/2001WR000355>, 2002.
- Droppers, B., Franssen, W. H. P., van Vliet, M. T. H., Nijssen, B., and Ludwig, F.: Simulating human impacts on global water resources using VIC-5, *Geosci. Model Dev.*, 13, 5029–5052, <https://doi.org/10.5194/gmd-13-5029-2020>, 2020.
- Eisner, S. and Flörke, M.: Benchmarking the WaterGAP3 global hydrology model in reproducing streamflow characteristics, *Geophysical Research Abstracts*, 17, EGU2015-11049, EGU General Assembly, 2015.
- Flörke, M., Kynast, E., Bärlund, I., Eisner, S., Wimmer, F., and Alcamo, J.: Domestic and industrial water uses of the past 60 years as a mirror of socio-economic development: A global simulation study, *Global. Environ. Chang.*, 23, 144–156, <https://doi.org/10.1016/j.gloenvcha.2012.10.018>, 2013.
- Gerten, D., Heck, V., Jägermeyr, J., Bodirsky, B. L., Fetzer, I., Jalava, M., Kummu, M., Lucht, W., Rockström, J., Schaphoff, S., and Schellnhuber, H. J.: Feeding ten billion people is possible within four terrestrial planetary boundaries, *Nature Sustainability*, 3, 200–208, <https://doi.org/10.1038/s41893-019-0465-1>, 2020.
- Hanasaki, N.: Code and data of Toward hyper-resolution global hydrological models including human activities: application to Kyushu Island, Japan, Zenodo [code and data set], <https://doi.org/10.5281/zenodo.5523280>, 2021.
- Hanasaki, N., Kanae, S., and Oki, T.: A reservoir operation scheme for global river routing models, *J. Hydrol.*, 327, 22–41, <https://doi.org/10.1016/j.jhydrol.2005.11.011>, 2006.
- Hanasaki, N., Kanae, S., Oki, T., Masuda, K., Motoya, K., Shirakawa, N., Shen, Y., and Tanaka, K.: An integrated model for the assessment of global water resources – Part 1: Model description and input meteorological forcing, *Hydrol. Earth Syst. Sci.*, 12, 1007–1025, <https://doi.org/10.5194/hess-12-1007-2008>, 2008a.
- Hanasaki, N., Kanae, S., Oki, T., Masuda, K., Motoya, K., Shirakawa, N., Shen, Y., and Tanaka, K.: An integrated model for the assessment of global water resources – Part 2: Applications and assessments, *Hydrol. Earth Syst. Sci.*, 12, 1027–1037, <https://doi.org/10.5194/hess-12-1027-2008>, 2008b.
- Hanasaki, N., Inuzuka, T., Kanae, S., and Oki, T.: An estimation of global virtual water flow and sources of water withdrawal for major crops and livestock products using a global hydrological model, *J. Hydrol.*, 384, 232–244, <https://doi.org/10.1016/j.jhydrol.2009.09.028>, 2010.
- Hanasaki, N., Yoshikawa, S., Kakinuma, K., and Kanae, S.: A seawater desalination scheme for global hydrological models, *Hydrol. Earth Syst. Sci.*, 20, 4143–4157, <https://doi.org/10.5194/hess-20-4143-2016>, 2016.
- Hanasaki, N., Yoshikawa, S., Pokhrel, Y., and Kanae, S.: A Quantitative Investigation of the Thresholds for Two Conventional Water Scarcity Indicators Using a State-of-the-Art Global Hydrological Model With Human Activities, *Water Resour. Res.*, 54, 8279–8294, <https://doi.org/10.1029/2018WR022931>, 2018a.
- Hanasaki, N., Yoshikawa, S., Pokhrel, Y., and Kanae, S.: A global hydrological simulation to specify the sources of water used by humans, *Hydrol. Earth Syst. Sci.*, 22, 789–817, <https://doi.org/10.5194/hess-22-789-2018>, 2018b.
- Harris, I., Jones, P. D., Osborn, T. J., and Lister, D. H.: Updated high-resolution grids of monthly climatic observations – the CRU TS3.10 Dataset, *Int. J. Climatol.*, 34, 623–642, <https://doi.org/10.1002/joc.3711>, 2014.
- Hersbach, H., Bell, B., Berrisford, P., Hirahara, S., Horányi, A., Muñoz-Sabater, J., Nicolas, J., Peubey, C., Radu, R., Schepers, D., Simmons, A., Soci, C., Abdalla, S., Abellan, X., Balsamo, G., Bechtold, P., Biavati, G., Bidlot, J., Bonavita, M., De Chiara, G., Dahlgren, P., Dee, D., Diamantakis, M., Dragani, R., Flemming, J., Forbes, R., Fuentes, M., Geer, A., Haimberger, L., Healy, S., Hogan, R. J., Hólm, E., Janisková, M., Keeley, S., Laloyaux, P., Lopez, P., Lupu, C., Radnoti, G., de Rosnay, P., Rozum, I., Vamborg, F., Villaume, S., and Thépaut, J.-N.: The ERA5 global reanalysis, *Q. J. Roy. Meteor. Soc.*, 146, 1999–2049, <https://doi.org/10.1002/qj.3803>, 2020.
- Japan Water Works Association (JWWA): Water works statistics 2016, Japan Water Works Association, 2018.
- Ji, P., Yuan, X., and Liang, X.-Z.: Do Lateral Flows Matter for the Hyperresolution Land Surface Modeling?, *J. Geophys. Res.-Atmos.*, 122, 12077–12092, <https://doi.org/10.1002/2017JD027366>, 2017.
- Kohyama, K., Hojito, M., Sasaki, H., and Miyaji, H.: Generation of Agricultural Statistics Mesh Data Using Digital National Land Information, Japanese Society of Soil Science and Plant Nutrition, 74, 415–424, 2003.
- Kondo, J.: Meteorology of water environment, Asakura Publishing, Tokyo, Japan, ISBN 978-4-254-16110-6, 1994.
- Kotsuki, S. and Tanaka, K.: SACRA – a method for the estimation of global high-resolution crop calendars from a satellite-sensed NDVI, *Hydrol. Earth Syst. Sci.*, 19, 4441–4461, <https://doi.org/10.5194/hess-19-4441-2015>, 2015.
- Kumamoto City: A world-class pure groundwater city Kumamoto, Japan, https://www.city.kumamoto.jp/kankyo/hpkiji/pub/Detail.aspx?c_id=5&id=20548 (last access: 7 July 2021), 2015.

- Masaki, Y., Hanasaki, N., Biemans, H., Müller Schmied, H., Tang, Q., Wada, Y., Gosling, S. N., Takahashi, K., and Hijioka, Y.: Intercomparison of global river discharge simulations focusing on dam operation—multiple models analysis in two case-study river basins, Missouri–Mississippi and Green–Colorado, *Environ. Res. Lett.*, 12, 055002, <https://doi.org/10.1088/1748-9326/aa57a8>, 2017.
- Masood, M., Yeh, P. J.-F., Hanasaki, N., and Takeuchi, K.: Model study of the impacts of future climate change on the hydrology of Ganges–Brahmaputra–Meghna basin, *Hydrol. Earth Syst. Sci.*, 19, 747–770, <https://doi.org/10.5194/hess-19-747-2015>, 2015.
- Mateo, C. M., Hanasaki, N., Komori, D., Tanaka, K., Kiguchi, M., Champathong, A., Sukhapunnaphan, T., Yamazaki, D., and Oki, T.: Assessing the impacts of reservoir operation to floodplain inundation by combining hydrological, reservoir management, and hydrodynamic models, *Water Resour. Res.*, 50, 7245–7266, <https://doi.org/10.1002/2013wr014845>, 2014.
- McDonald, R. I., Weber, K., Padowski, J., Flörke, M., Schneider, C., Green, P. A., Gleeson, T., Eckman, S., Lehner, B., Balk, D., Boucher, T., Grill, G., and Montgomery, M.: Water on an urban planet: Urbanization and the reach of urban water infrastructure, *Global. Environ. Chang.*, 27, 96–105, <https://doi.org/10.1016/j.gloenvcha.2014.04.022>, 2014.
- Ministry of Economy Trade and Industry (METI): Census of Manufactory Site and Water 2016, Ministry of Economy Trade and Industry (METI), Tokyo, Japan, <https://www.meti.go.jp/statistics/tyo/kougyo/> (last access: 11 April 2022), 2018.
- Ministry of Land Infrastructure Transportation and Tourism (MLIT): Present condition of water resources in Japan, Ministry of Land Infrastructure Transportation and Tourism (MLIT), Tokyo, Japan, 142, https://www.mlit.go.jp/mizukokudo/mizsei/mizukokudo_mizsei_fr1_000037.html (last access: 11 April 2022), 2021.
- Monfreda, C., Ramankutty, N., and Foley, J. A.: Farming the Planet. Part 2: The Geographic Distribution of Crop Areas and Yields in the Year 2000, *Glob. Biogeochem. Cy.*, 22, GB1022, <https://doi.org/10.1029/2007GB002947>, 2008.
- Müller Schmied, H., Cáceres, D., Eisner, S., Flörke, M., Herbert, C., Niemann, C., Peiris, T. A., Popat, E., Portmann, F. T., Reinecke, R., Schumacher, M., Shadkam, S., Telteu, C.-E., Trautmann, T., and Döll, P.: The global water resources and use model WaterGAP v2.2d: model description and evaluation, *Geosci. Model Dev.*, 14, 1037–1079, <https://doi.org/10.5194/gmd-14-1037-2021>, 2021.
- Nash, J. E. and Sutcliffe, J. V.: River flow forecasting through conceptual models part I – A discussion of principles, *J. Hydrol.*, 10, 282–290, [https://doi.org/10.1016/0022-1694\(70\)90255-6](https://doi.org/10.1016/0022-1694(70)90255-6), 1970.
- Oki, T., Valeo, C., and Heal, K.: Hydrology 2020: An Integrating Science to Meet World Water Challenges, *IAHS Proceedings & Reports*, edited by: Oki, T., Valeo, C., and Heal, K., IAHS Press, Wallingford, UK, 190 pp., ISBN 978-1901502336, 2006.
- Pokhrel, Y., Hanasaki, N., Koira, S., Cho, J., Yeh, P. J. F., Kim, H., Kanae, S., and Oki, T.: Incorporating Anthropogenic Water Regulation Modules into a Land Surface Model, *J. Hydrometeorol.*, 13, 255–269, <https://doi.org/10.1175/jhm-d-11-013.1>, 2012.
- Ramankutty, N., Evan, A., Monfreda, C., and Foley, J. A.: Farming the Planet. Part 1: The Geographic Distribution of Global Agricultural Lands in the Year 2000, *Glob. Biogeochem. Cy.*, 22, GB1003, <https://doi.org/10.1029/2007GB002952>, 2008.
- Rost, S., Gerten, D., Bondeau, A., Lucht, W., Rohwer, J., and Schaphoff, S.: Agricultural green and blue water consumption and its influence on the global water system, *Water Resour. Res.*, 44, W09405, <https://doi.org/10.1029/2007WR006331>, 2008.
- Schaphoff, S., von Bloh, W., Rammig, A., Thonicke, K., Biemans, H., Forkel, M., Gerten, D., Heinke, J., Jägermeyr, J., Knauer, J., Langerwisch, F., Lucht, W., Müller, C., Rolinski, S., and Waha, K.: LPJmL4 – a dynamic global vegetation model with managed land – Part 1: Model description, *Geosci. Model Dev.*, 11, 1343–1375, <https://doi.org/10.5194/gmd-11-1343-2018>, 2018.
- Schewe, J., Heinke, J., Gerten, D., Haddeland, I., Arnell, N. W., Clark, D. B., Dankers, R., Eisner, S., Fekete, B. M., Colón-González, F. J., Gosling, S. N., Kim, H., Liu, X., Masaki, Y., Portmann, F. T., Satoh, Y., Stacke, T., Tang, Q., Wada, Y., Wisser, D., Albrecht, T., Frieler, K., Piontek, F., Warszawski, L., and Kabat, P.: Multimodel assessment of water scarcity under climate change, *P. Natl. Acad. Sci. USA*, 111, 3245–3250, <https://doi.org/10.1073/pnas.1222460110>, 2014.
- Schneider, U., Becker, A., Finger, P., Meyer-Christoffer, A., Ziese, M., and Rudolf, B.: GPCP’s new land surface precipitation climatology based on quality-controlled in situ data and its role in quantifying the global water cycle, *Theor. Appl. Climatol.*, 115, 15–40, <https://doi.org/10.1007/s00704-013-0860-x>, 2014.
- Shin, S., Pokhrel, Y., and Miguez-Macho, G.: High-Resolution Modeling of Reservoir Release and Storage Dynamics at the Continental Scale, *Water Resour. Res.*, 55, 787–810, <https://doi.org/10.1029/2018wr023025>, 2019.
- Shumilova, O., Tockner, K., Thieme, M., Koska, A., and Zarfl, C.: Global Water Transfer Megaprojects: A Potential Solution for the Water-Food-Energy Nexus?, *Front. Environ. Sci.*, 6, 150, <https://doi.org/10.3389/fenvs.2018.00150>, 2018.
- Siebert, S., Döll, P., Hoogeveen, J., Faures, J.-M., Frenken, K., and Feick, S.: Development and validation of the global map of irrigation areas, *Hydrol. Earth Syst. Sci.*, 9, 535–547, <https://doi.org/10.5194/hess-9-535-2005>, 2005.
- Siebert, S., Burke, J., Faures, J. M., Frenken, K., Hoogeveen, J., Döll, P., and Portmann, F. T.: Groundwater use for irrigation – a global inventory, *Hydrol. Earth Syst. Sci.*, 14, 1863–1880, <https://doi.org/10.5194/hess-14-1863-2010>, 2010.
- Statistic Bureau of Japan: Grid Square Statistics of 2015 Population Census 2015, https://www.stat.go.jp/data/mesh/h27_w.html (last access: 11 April 2022), 2017.
- Sutanudjaja, E. H., van Beek, R., Wanders, N., Wada, Y., Bosmans, J. H. C., Drost, N., van der Ent, R. J., de Graaf, I. E. M., Hoch, J. M., de Jong, K., Karssenber, D., López López, P., Peßenteiner, S., Schmitz, O., Straatsma, M. W., Vannamete, E., Wisser, D., and Bierkens, M. F. P.: PCR-GLOBWB 2: a 5 arcmin global hydrological and water resources model, *Geosci. Model Dev.*, 11, 2429–2453, <https://doi.org/10.5194/gmd-11-2429-2018>, 2018.
- Turner, S. W. D., Xu, W., and Voisin, N.: Inferred inflow forecast horizons guiding reservoir release decisions across the United States, *Hydrol. Earth Syst. Sci.*, 24, 1275–1291, <https://doi.org/10.5194/hess-24-1275-2020>, 2020.
- van Dijk, A. I. J. M., Peña-Arancibia, J. L., Wood, E. F., Sheffield, J., and Beck, H. E.: Global analysis of seasonal streamflow predictability using an ensemble prediction system and observations from 6192 small catchments worldwide, *Water Resour. Res.*, 49, 2729–2746, <https://doi.org/10.1002/wrcr.20251>, 2013.

- Wada, Y., van Beek, L. P. H., van Kempen, C. M., Reckman, J. W. T. M., Vasak, S., and Bierkens, M. F. P.: Global depletion of groundwater resources, *Geophys. Res. Lett.*, 37, L20402, <https://doi.org/10.1029/2010GL044571>, 2010.
- Wada, Y., van Beek, L. P. H., Viviroli, D., Dürr, H. H., Weingartner, R., and Bierkens, M. F. P.: Global monthly water stress: 2. Water demand and severity of water stress, *Water Resour. Res.*, 47, W07518, <https://doi.org/10.1029/2010wr009792>, 2011.
- Wada, Y., Wisser, D., Eisner, S., Flörke, M., Gerten, D., Haddeland, I., Hanasaki, N., Masaki, Y., Portmann, F. T., Stacke, T., Tessler, Z., and Schewe, J.: Multi-model projections and uncertainties of irrigation water demand under climate change, *Geophys. Res. Lett.*, 40, 4626–4632, <https://doi.org/10.1002/grl.50686>, 2013.
- Wada, Y., de Graaf, I. E. M., and van Beek, L. P. H.: High-resolution modeling of human and climate impacts on global water resources, *J. Adv. Model. Earth Sy.*, 8, 735–763, <https://doi.org/10.1002/2015MS000618>, 2016.
- Weedon, G. P., Balsamo, G., Bellouin, N., Gomes, S., Best, M. J., and Viterbo, P.: The WFDEI meteorological forcing data set: WATCH Forcing Data methodology applied to ERA-Interim reanalysis data, *Water Resour. Res.*, 50, 7505–7514, <https://doi.org/10.1002/2014WR015638>, 2014.
- Wood, E. F., Roundy, J. K., Troy, T. J., van Beek, L. P. H., Bierkens, M. F. P., Blyth, E., de Roo, A., Döll, P., Ek, M., Famiglietti, J., Gochis, D., van de Giesen, N., Houser, P., Jaffé, P. R., Kollet, S., Lehner, B., Lettenmaier, D. P., Peters-Lidard, C., Sivapalan, M., Sheffield, J., Wade, A., and Whitehead, P.: Hyper-resolution global land surface modeling: Meeting a grand challenge for monitoring Earth’s terrestrial water, *Water Resour. Res.*, 47, <https://doi.org/10.1029/2010WR010090>, 2011.
- Wisser, D., Fekete, B. M., Vörösmarty, C. J., and Schumann, A. H.: Reconstructing 20th century global hydrography: a contribution to the Global Terrestrial Network-Hydrology (GTN-H), *Hydrol. Earth Syst. Sci.*, 14, 1–24, <https://doi.org/10.5194/hess-14-1-2010>, 2010.
- Yamazaki, D., Oki, T., and Kanae, S.: Deriving a global river network map and its sub-grid topographic characteristics from a fine-resolution flow direction map, *Hydrol. Earth Syst. Sci.*, 13, 2241–2251, <https://doi.org/10.5194/hess-13-2241-2009>, 2009.
- Yamazaki, D., Ikeshima, D., Tawatari, R., Yamaguchi, T., O’Loughlin, F., Neal, J. C., Sampson, C. C., Kanae, S., and Bates, P. D.: A high-accuracy map of global terrain elevations, *Geophys. Res. Lett.*, 44, 5844–5853, <https://doi.org/10.1002/2017GL072874>, 2017.
- Yamazaki, D., Ikeshima, D., Sosa, J., Bates, P. D., Allen, G. H., and Pavelsky, T. M.: MERIT Hydro: A High-Resolution Global Hydrography Map Based on Latest Topography Dataset, *Water Resour. Res.*, 55, 5053–5073, <https://doi.org/10.1029/2019WR024873>, 2019.
- Yassin, F., Razavi, S., Elshamy, M., Davison, B., Sapriza-Azuri, G., and Wheater, H.: Representation and improved parameterization of reservoir operation in hydrological and land-surface models, *Hydrol. Earth Syst. Sci.*, 23, 3735–3764, <https://doi.org/10.5194/hess-23-3735-2019>, 2019.
- Yatagai, A., Kamiguchi, K., Arakawa, O., Hamada, A., Yasutomi, N., and Kitoh, A.: APHRODITE: Constructing a Long-Term Daily Gridded Precipitation Dataset for Asia Based on a Dense Network of Rain Gauges, *B. Am. Meteorol. Soc.*, 93, 1401–1415, 2012.
- Yoshida, T., Hanasaki, N., Nishina, K., Boulange, J., Okada, M., and Troch, P. A.: Inference of Parameters for a Global Hydrological Model: Identifiability and Predictive Uncertainties of Climate-Based Parameters, *Water Resour. Res.*, 58, e2021WR030660, <https://doi.org/10.1029/2021WR030660>, 2022.